CityU Scholars

B-Site Doping of Metal Halide Perovskite Nanoplatelets Influences Their Optical Properties

Litvin, Aleksandr P.; Margaryan, Igor V.; Yin, Wenxu; Zhang, Xiayou; Zheng, Weitao; Rogach, Andrey L.

Published in:
Advanced Optical Materials

Published: 14/03/2024

Document Version:
Post-print, also known as Accepted Author Manuscript, Peer-reviewed or Author Final version

Publication record in CityU Scholars:
Go to record

Published version (DOI):
10.1002/adom.202301001

Publication details:
Litvin, A. P., Margaryan, I. V., Yin, W., Zhang, X., Zheng, W., & Rogach, A. L. (2024). B-Site Doping of Metal Halide Perovskite Nanoplatelets Influences Their Optical Properties. *Advanced Optical Materials*, *12*(8), Article 2301001. https://doi.org/10.1002/adom.202301001

Citing this paper
Please note that where the full-text provided on CityU Scholars is the Post-print version (also known as Accepted Author Manuscript, Peer-reviewed or Author Final version), it may differ from the Final Published version. When citing, ensure that you check and use the publisher's definitive version for pagination and other details.

General rights
Copyright for the publications made accessible via the CityU Scholars portal is retained by the author(s) and/or other copyright owners and it is a condition of accessing these publications that users recognise and abide by the legal requirements associated with these rights. Users may not further distribute the material or use it for any profit-making activity or commercial gain.

Publisher permission
Permission for previously published items are in accordance with publisher's copyright policies sourced from the SHERPA RoMEO database. Links to full text versions (either Published or Post-print) are only available if corresponding publishers allow open access.

Take down policy
Contact lbscholars@cityu.edu.hk if you believe that this document breaches copyright and provide us with details. We will remove access to the work immediately and investigate your claim.

Download date: 20/03/2025

This is the accepted version of the following article: Litvin, A. P., Margaryan, I. V., Yin, W., & Zhang, X. et al. (2023). B-Site Doping of Metal Halide Perovskite Nanoplatelets Influences Their Optical Properties. *Advanced Optical Materials*, Article 2301001, advanced online publication, which has been published in final form at https://doi.org/10.1002/adom.202301001. This article may be used for non-commercial purposes in accordance with Wiley Terms and Conditions for Use of Self-Archived Versions. This article may not be enhanced, enriched or otherwise transformed into a derivative work, without express permission from Wiley or by statutory rights under applicable legislation. Copyright notices must not be removed, obscured or modified. The article must be linked to Wiley's version of record on Wiley Online Library and any embedding, framing or otherwise making available the article or pages thereof by third parties from platforms, services and websites other than Wiley Online Library must be prohibited.

B-Site Doping of Metal Halide Perovskite Nanoplatelets Influences Their Optical Properties

Aleksandr P. Litvin,[1*] Igor V. Margaryan,[2] Wenxu Yin,[1] Xiayou Zhang,[1] Weitao Zheng[1], Andrey L. Rogach[3*]

[1]Key Laboratory of Automobile Materials MOE, School of Materials Science & Engineering, and Jilin Provincial International Cooperation Key Laboratory of High-Efficiency Clean Energy Materials, Jilin University, Changchun, 130012, P. R. China

[2]PhysNano Department, ITMO University, Saint Petersburg, 197101 Russia

[3]Department of Materials Science and Engineering, and Centre for Functional Photonics (CFP), City University of Hong Kong, 83 Tat Chee Avenue, Hong Kong S.A.R., 999077 P. R. China

*Corresponding authors. litvin88@gmail.com (APL); andrey.rogach@cityu.edu.hk (ALR)

Abstract

Metal halide perovskite nanoplatelets (NPls) have recently joined a rich family of 2D semiconductor nanomaterials. Quantum and dielectric confinement in these nanostructures endow them with useful optical properties, which include, but are not limited to, high linear and nonlinear absorption coefficients, narrow and tunable emission bands, and high photoluminescence quantum yield. These characteristics render perovskite NPls promising for applications in lightning, photodetection, nonlinear optics, and photocatalysis. Doping is a universal approach for tuning optical and electronic properties of semiconductor materials, and the B-site doping of perovskite NPls allows us to further improve and adjust on demand their above-mentioned optical properties and may result in the appearance of fundamentally new behavior through embedding optically active dopants. In this mini-review, we shortly summarize the basic knowledge about perovskite NPls in terms of their colloidal synthesis, and then consider the B-site doping of perovskite NPls in terms of the existing approaches (in-situ and post-synthetic doping) and its effect on their optical characteristics (doping with self-emitting ions such as Mn^{2+} and rare-earth elements; consequences for the nonlinear optical response).

Keywords: metal halide perovskites, nanoplatelets, doping, photoluminescence, nonlinear optics

ToC image

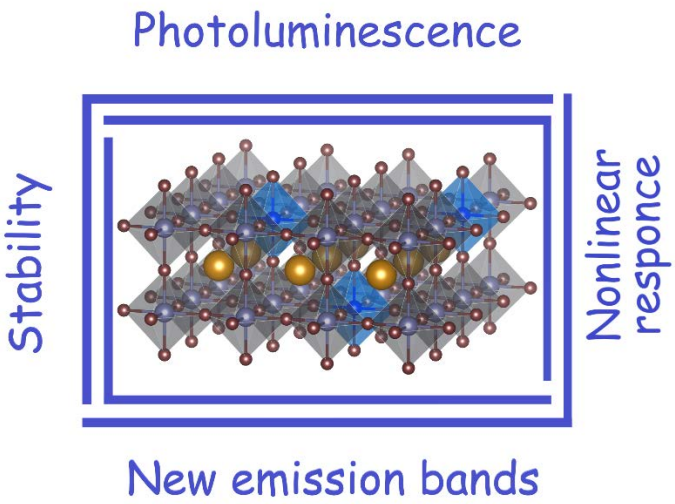

ToC text

Metal halide perovskite nanoplatelets possess high linear and nonlinear absorption coefficients, narrow and tunable emission bands, and high photoluminescence quantum yield. This makes them promising for applications in lightning, photodetection, nonlinear optics, and photocatalysis. B-site doping of perovskite nanoplatelets is a versatile strategy to improve or modify their attractive properties, as considered in this mini-review.

1. Introduction

Metal halide perovskites described by general structural formula ABX_3, where the A-site is occupied by organic or inorganic cation (typically, methylammonium (MA^+), formamidinium (FA^+), or Cs^+, B-site – by a divalent metal cation (Pb^{2+}, Sn^{2+}, Ge^{2+}, etc.), and X-site – by a halide anion (Cl^-, Br^-, I^-) have attracted much attention in recent years due to their promising optical properties, especially, when produced in the form of colloidal nanoparticles by chemical synthesis in solution. The simplicity and variability of their colloidal synthesis combined with customizable optical properties stimulate plenty of research in the field of perovskite nanostructures. Perovskite nanoplatelets (NPls) are two-dimensional (2D) colloidal materials with confinement in only one dimension, as their thickness is typically smaller than the exciton Bohr radius of the corresponding bulk material. Thus, the charge carriers in NPls experience strong 1D quantum confinement, which manifests itself in a significant blue shift of their absorption and photoluminescence (PL) spectra, depending on the NPl thickness (Figure 1a). While the control over the NPl thickness allows us to vary the position of the emission bands over the wide spectral range, similar to other halide perovskites changes in the chemical composition through post-synthetic halide exchange is another tool for the adjustment of the emission wavelength (Figure 1b). There are several theoretical models approbated to describe the bandgap energy landscape in 2D perovskite NPls (Figure 1c): an infinite quantum well model, a two-step infinite quantum model (takes ligands into account), and a Kronig-Penny model (takes NPls stacking into account). Figure 1d provides the comparison of the experimentally determined bandgap energies (square symbols) for 2D perovskite NPls ranging from 1 to 5 monolayers (ML) in thickness with above mentioned theoretical predictions. The best fitting ("full model") additionally accounts for a change in the exciton binding energy arising from the reduced dielectric screening effect. Besides, the precise control of the NPls thickness resulted in ultra-narrow PL bands (typically, full width at half maximum is below 20 nm) yielding superior color purity.[1–3]

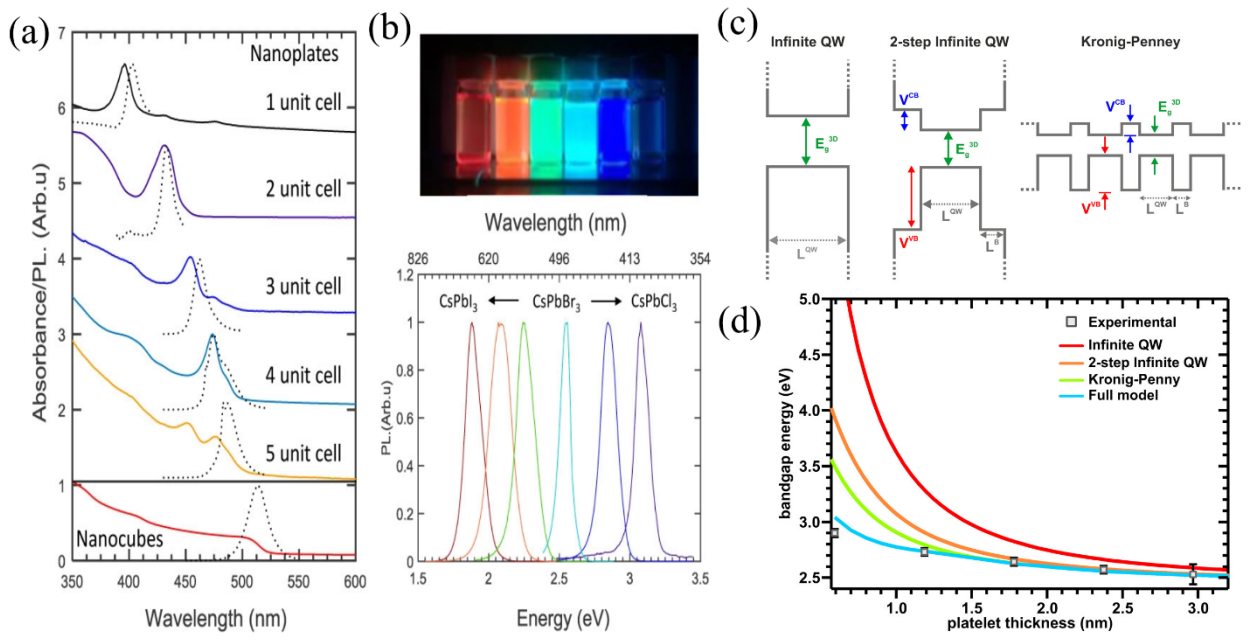

Figure 1. (a) Control over $CsPbBr_3$ NPls thickness allows for tuning of absorption and PL bands, which are all blue-shifted as compared with 3D nanocubes due to the quantum confinement effect. (b) Photographs and corresponding PL spectra of the colloidal dispersions of $CsPb(Br/I)_3$ and $CsPb(Cl/Br)_3$ NPls obtained by anion (halide) exchange Reproduced with permission.[4] Copyright 2015, American Chemical Society. (c) Theoretical models approbated to describe the bandgap energy landscape in 2D perovskite NPls: an infinite quantum well model, a two-step infinite quantum model (takes ligands into account), and a Kronig-Penny model (takes NPls stacking into account). (d) Comparison of the experimentally determined bandgap energies (square symbols) for 1-5 monolayered 2D perovskite NPls with above mentioned theoretical predictions. The best fitting ("full model") additionally accounts for a change in the exciton binding energy arising from the reduced dielectric screening. Reproduced with permission.[5] Copyright 2015, American Chemical Society.

Doping is a universal approach for tuning optical and electronic properties of semiconductors. For metal halide perovskites, B-site doping is an indispensable strategy to finely tune their optical and electronic properties, to stabilize their crystalline phases, and to introduce additional emission bands. Moreover, many efforts were made to replace toxic Pb^{2+} by isovalent doping or alloying with more environmentally friendly divalent cations. The most common example is the partial or complete replacement of lead(II) ions with tin(II) ions.[6–8] Despite some progress in this direction, the optoelectronic properties of such nanostructures are still inferior to those of lead-based perovskites. The introduction of other divalent cations with a smaller ionic radius was considered as a promising strategy for tuning the tolerance factor of perovskite lattice, which is especially important for the stabilization of the α-phase of the iodine-based perovskite nanostructures. Great progress in terms of increasing the luminescence efficiency, stability, and operational characteristics of optoelectronic devices based on $CsPbI_3$ perovskite nanocrystals was achieved by introduction of Sr^{2+},[9,10] Ni^{2+},[11] Ca^{2+},[12] and Zn^{2+} [13] cations. Besides, similar results were achieved through employing heterovalent doping of $CsPbI_3$ perovskite nanocrystals with smaller Sb^{3+},[14] Yb^{3+},[15] Gd^{3+},[16] or La^{3+} [17] cations. At the same time, the B-site doping perovskites with optically active ions such as Mn^{2+},[18,19] Yb^{3+},[20,21] Er^{3+},[22,23] etc. allows us to introduce additional emission bands, thus expanding their utilization in photonics and optoelectronics. In the latter case, perovskites serve as a matrix with high values of absorption cross-section leading to a strong sensitization of the dopants through internal photoexcitation transfer. Thus, the B-site doping includes many strategies for the modification of perovskite nanostructures.

As compared to the 0D perovskite nanocrystals, doping perovskite NPls is still in its infancy. Despite the aims and strategies being similar, brittle nature of perovskite NPls and their peculiar growth mechanisms should be taken into account. For instance, introducing additional cation sources during the synthesis may or may not be accompanied by doping of the formed nanostructures. In this regard, post-synthetic treatments, which induce partial cation substitution, provide man additional way for adjusting optical and electronic properties of perovskite NPls. Successful B-site doping of perovskite NPls can help to improve their photoluminescence quantum

yield (PL QY), stability, and nonlinear optical response. As a result, several recent studies reported on positive effect of doping on the efficiency and stability of NPls-based optoelectronic devices such as light-emitting diodes[24,25] (LEDs) and photodetectors.[26] In this mini-review, we briefly discuss the synthesis of colloidal ligands-stabilized NPls, and then consider doping of their B-site cations, paying special attention to the control over their morphology and optical properties. For more detailed information about synthesis, properties, and applications of the NPLs, we refer the interested reader to several recent reviews.[3,27–30]

2. Synthesis of NPls

Ligand-assisted reprecipitation (LARP)[31] and hot-injection synthesis[32] are the most widely used approaches to synthesize 2D perovskite NPls.[2] Initially, Tyagi et al. recognized $MAPbBr_3$ NPls as a side product in the LARP synthesis of perovskite nanocrystals.[33] Further purification of the reaction products led to separation of predominantly monolayered NPls. Sichert et al. intentionally prepared a series of $MAPbBr_3$ NPls, exercising their thickness control (Figure 2a).[5] Soon after that, a modified LARP process yielding fully inorganic $CsPbBr_3$ NPls was introduced by Akkerman et al.[34] Levchuk et al. demonstrated the thickness-tunable synthesis of $MAPbBr_3$, $MAPbI_3$, $FAPbBr_3$, and $FAPbCl_3$ NPls, where an increase of oleylamine (OlAm) / oleic acid (OA) ratio led to reducing NPls thickness.[35,36] To date, a careful choice of antisolvents,[36,37] A-to-B cations ratio,[38,39] type and amount of ligands,[35,36,40] and additives[34,41] allow for the fine control over the NPls synthesis using LARP approach.

Hot-injection method (Figure 2b), which typically implies an injection of initially prepared monovalent cation precursor into a metal halide precursor solution at a certain temperature under inert atmosphere, was adopted for the synthesis of fully-inorganic[4] and organic-inorganic[42] perovskite NPls. Besides the thickness control, the control of lateral dimensions was achieved by adjusting the reaction temperature, ligands type, and their ratio. Ligand concentration,[43] length of ligand chains,[44,45] and use of additional metal cations[25,46] also played a role in maintaining a 2D shape.

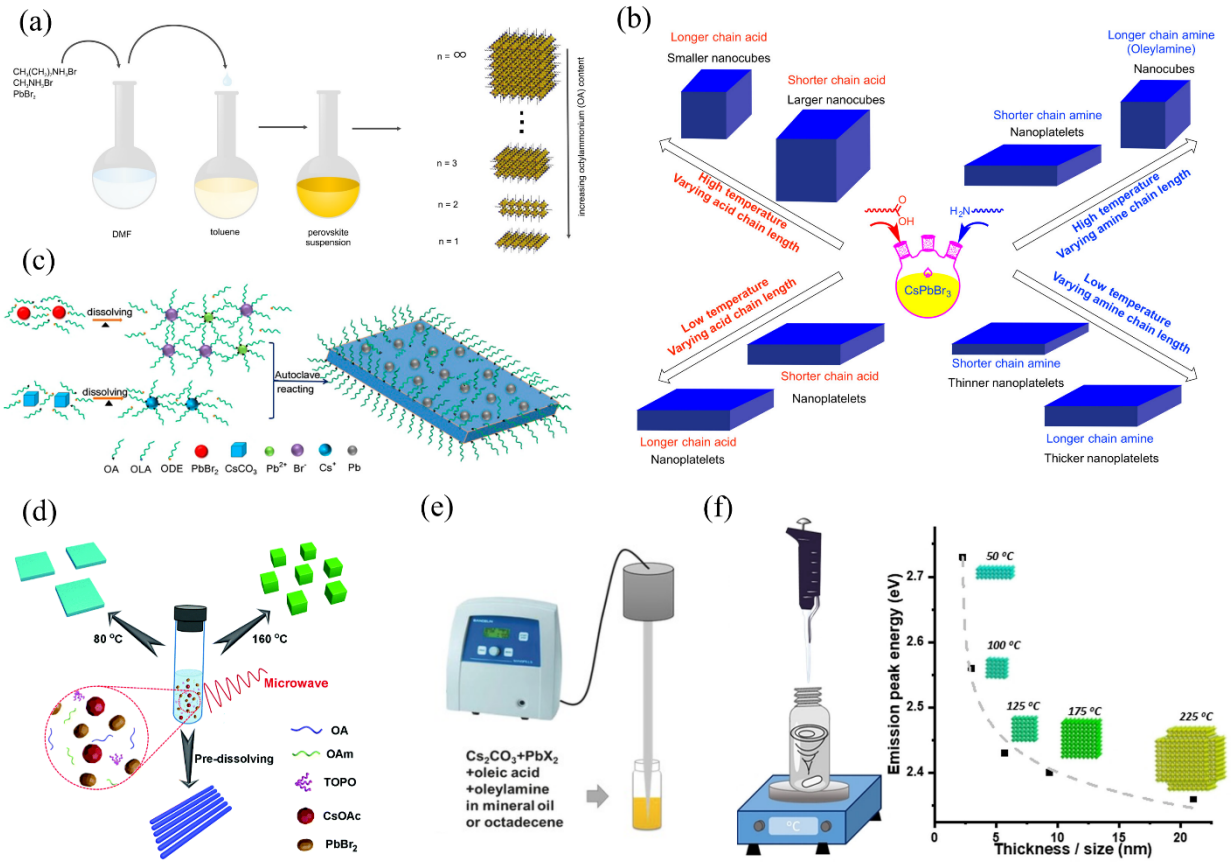

Figure 2. Illustration of different synthetic approaches for producing perovskite NPls. (a) LARP synthesis is based on the injection of perovskite precursors and ligands (octylammonium bromide (OctAm-Br), methylammonium bromide (MA-Br), and $PbBr_2$) dispersed in DMF ("good solvent") into toluene ("poor solvent"), which is resulted in immediate supersaturation and drives the growth of perovskite NPls. Thickness control was achieved by variation of OctAm-to-{OctAm+MA} ratio Reproduced with permission.[5] Copyright 2015, American Chemical Society. (b) Hot-injection method is based on high-temperature (typically, 140−170 °C) injection of the initially prepared Cs-oleate or Cs-acetate into a mixture of B- and X-ion precursors and ligands in octadecene (ODE) solvent under inert atmosphere. The size and shape evolution of resulting nanocubes and NPls is achieved by variation of the hydrocarbon chain length of carboxylic acids and amines. Reproduced with permission.[44] Copyright 2016, American Chemical Society. (c) Solvothermal synthesis of $CsPbBr_3$ NPls by the interaction of pre-dissolved precursors and ligands in an autoclave. The control of morphology was realized through variation of temperature and time of the reaction. Reproduced with permission.[47] Copyright 2018, American Chemical Society. (d) Microwave-assisted reaction between perovskite precursors and ligands yields $CsPbBr_3$ nanostructures of different morphology, depending on how precursors were dissolved and the temperature of the reaction. Reproduced with permission.[48] Copyright 2017, Royal Society of Chemistry. (e) Synthesis of perovskite nanostructures by tip-ultrasonication of precursor salts (Cs_2CO_3 and $PbBr_2$) and ligands in a nonpolar solvent. Anisotropic growth and thickness control were achieved by a reduction of Cs_2CO_3 content. Reproduced with permission.[49] Copyright 2016, Wiley-VCH. (f) Inert gas-free hot injection of the pre-heated Cs-oleate precursor into dissolved lead halide precursor and ligands. A reduction of temperature of lead halide precursor during injection yielded 2D perovskite NPls. Reproduced with permission.[50] Copyright 2021, Wiley-VCH.

Apart from these two commonly used synthetic approaches, several other alternative techniques have been proposed. One of them is a solvothermal synthesis of perovskite NPls using an autoclave (Figure 2c). Chen et al.[51] have reported a solvothermal synthesis of lead halide perovskite nanostructures as a strategy to obtain both nanocubes and nanowires with a high photoluminescence quantum yield (PL QY) and uniformity. Soon after that, Zhai et al.[47] reported a solvothermal method to produce inorganic perovskite NPls. In a typical synthesis (Figure 2c), initially prepared Cs-oleate and $PbBr_2$ precursors were loaded into an autoclave, and the reaction rate was controlled by time and temperature. This approach brought a high yield of NPls in the chemical reaction, while PL QY of 7-ML NPls reached 50%. Chen and et al.[52] further exercised the morphology control over the products of solvothermal reaction to produce perovskite nanostructures in the form of 3D nanocubes, 2D nanoplatelets/nanoribbons, and 1D nanorods. A gradual decrease in Cs precursor amount induced change in the morphology, while Cs deficiency at the perovskite surface was compensated by octylammonium ions acting as cations, further promoting anisotropic growth. Zhang et al. varied a solvothermal reaction time to control both lateral dimensions and a thickness of $CsPbCl_3$ NPls.[53] Xie et al.[54] reported pure-red emissive $CsPbI_3$ NPls obtained by a solvothermal method. Parveen et al.[55] illustrated solvothermal synthesis of organic-inorganic $MAPbBr_3$ multilayer-to-bilayer nanosheets, where increasing reaction temperature induced the shape evolution from nanorods to nanosheets.

Besides, several other approaches for NPls synthesis, such as tip-ultrasonication,[49] ligand-assisted exfoliation,[56] room-temperature injection followed with heating up[57] or heating up exclusively,[58–60] inert gas-free hot-injection,[50] ligand-assisted exfoliation,[61] and microwave-assisted synthesis[48] have been demonstrated; some of them are illustrated in Figure 2d-f.

3. B-site doping

Generally, doping strategies of nanostructures can be divided into two main categories: *in-situ* (introduction of the dopant precursors during the synthesis) and *ex-situ* (post-synthetic partial cation exchange) procedures. Within the first approach, various precursors were tested as sources of the guest cations during hot-injection, LARP, solvothermal, or ultrasonication synthesis of perovskite nanostructures. In an early work, Liu et al. reported that both the nature of the dopant precursor and that of the host are essential for successful perovskite doping.[18] They claimed that close energies of Mn-Cl and Pb-Cl bond dissociation should favor successful doping and formation of Mn^{2+}:$CsPbCl_3$ nanocrystals. Later on, Chen et al. showed that bond dissociation energies should be considered together with a guest-cation size in order to explain the kinetics of the formation of doped/passivated perovskite nanocrystals.[62] Using X-ray photoelectron spectroscopy before and after nanocrystal etching, they demonstrated that different guest cations can be either incorporated into nanocrystals lattice, located at the surface, or no be present either in the core or at the surface. The knowledge of the exact location of the dopants is important for understanding the mechanism underlining further changes in perovskites' optical properties. While metal halide precursors were most widely used for in-situ doping, the role of doping can be masked by halide-rich conditions during the synthesis.[2] The solubility of the dopant precursors should also be taken into account

for the selection of chemical reactions. For instance, the poor solubility of $YbCl_3$ hydrates motivated Milstein et al. to use metal-acetate salts and chlorotrimethylsilane as the cation and halide precursors respectively to produce Yb^{3+}:$CsPbCl_3$ perovskite nanocrystals.[21] Huang et al. modified this approach by replacing metal-acetate salts with metal-oleates to avoid precipitation of precursors at a high temperature.[63]

Post-synthetic treatment is another way to introduce new B-site cations into lead-halide perovskite nanostructures. Van der Stam et al. proposed partial cation exchange (Pb^{2+} to Sn^{2+}, Cd^{2+}, and Zn^{2+}) using the metal bromide salts dissolved in toluene in the presence of OlAm.[64] They showed that the post-synthetic B-site doping could be applied for perovskite nanocrystals without deterioration of their shape, crystallinity, and optical properties. Importantly, they demonstrated that the dopant-induced blue shift of a PL peak position scales linearly with the lattice vector of the doped nanocrystals. These finding pawed the way for the further development of post-synthetic doping protocols with various precursors, solvents, and ligands, which all play a pivotal role during this process.

Both isovalent (Mn^{2+}[65–69], Ni^{2+} [70], Sn^{2+} [60], Cu^{2+} [25], Ba^{2+} [71], Zn^{2+} [25]) and heterovalent (Sn^{4+} [60,72], Ti^{4+} [60], Sb^{3+} [14,71], Eu^{3+} [25,71], Ce^{3+}, Tb^{3+} [73], Lu^{3+}, Nd^{3+}, Gd^{3+} [74], and Yb^{3+} [75,76]) cations have been introduced into perovskite NPls as B-site dopants by following the above mentioned approaches, as will be discussed in detail in the next subsections. First, in-situ and ex-situ approaches for perovskite NPls will be considered. Then, we will separately consider the doping with Mn^{2+} and Yb^{3+} ions, which leads to appearance of additional emission bands in perovskite nanostructures.

3.1 In-situ doping during the NPl synthesis

Before considering actual in-situ doping, we notice that in some cases introduction of additives during the synthesis of NPls changed the reaction kinetics but was not accompanied by doping. Sheng et al.[46] proposed a metal halide modulation approach to synthesize $CsPbX_3$ NPls, where their morphology changed from nanocubes to NPls to small irregular-shaped nanoparticles (Figure 3a) by varying the amount of additional metal halide such as $CuCl_2$, time and temperature of the chemical reaction, and ligands ratio. Both metal and halide ions from the additive substance were responsible for achieving specific morphology, while no evidence indicating occurrence of metal doping was found. Ding et al. developed a cation-mediated control over morphology using Sn^{2+} and Sn^{4+} ions during one-pot synthesis of $CsPbBr_3$ and $CsPbCl_xBr_{3-x}$ perovskites[60] They found out that the added cations were not inserted into the perovskite host but strongly altered chemical reaction kinetics. The comparison of the reaction conducted under an inert and open-air atmosphere implied that Sn^{4+} was responsible for the preferential growth of thin NPls. Two mechanisms were suggested to explain their lateral growth: Sn^{4+} ions acting as capping ligands and directing the growth; and Sn^{4+} ions forming bonds with OA or OlAm ligands which promoted their extraction from specific NPl facets, thus providing their higher reactivity. Indeed, Bonato et al. later showed that Sn^{4+} ions acting as hard Lewis acids are able to interact with OlAm,[72] leading to the formation of an adduct between Sn^{4+} and OlAm, changing of OA/OlAm acid-base

equilibrium and increasing the OlAm protonation rate, which promoted anisotropic growth of NPls (Figure 3b).

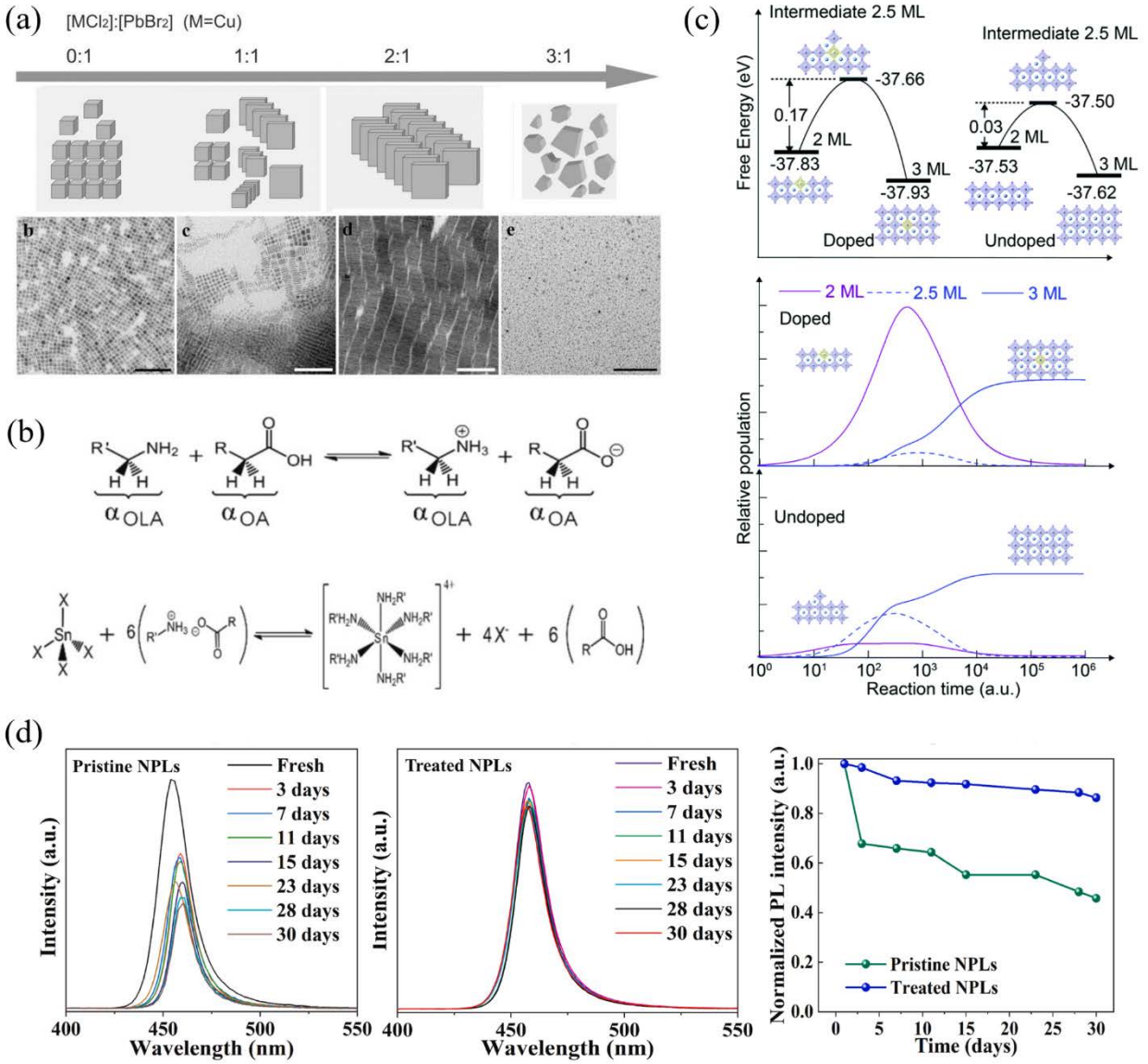

Figure 3. (a) An increase of the amount of $CuCl_2$ used as a modulator of chemical reaction changes morphology $CsPbX_3$ perovskites from nanocubes to NPls to small irregular shape nanoparticles, which is supported by TEM analysis, while no evidence indicating occurrence of metal doping was found. Reproduced with permission.[46] Copyright 2018, Wiley-VCH. (b) Acid-base equilibrium between OA and OlAm (upper panel) shifts towards OA due to formation of the adduct between SnX_4 and OlAm (lower panel). Reproduced with permission.[72] Copyright 2020, Wiley-VCH. (c) Lanthanide doping enlarges the energy barrier for the formation of intermediated 2.5-monolayered $CsPbBr_3$ NPls, thus changing the growth kinetics and offering a possibility to predominantly obtain metastable 2 ML NPls. Reproduced with permission.[74] Copyright 2021, Royal Society of Chemistry. (d) $NiBr_2$ passivation results in improved stability of $CsPbBr_3$ NPls, evaluated by respective PL spectra. Reproduced with permission.[24] Copyright 2023, Elsevier Ltd.

Several studies indicating successful incorporation of B-site dopants (still affecting the growth kinetics) have been reported, with characteristics of the resulting doped perovskite NPls listed in Table 1. Bera et al. studied Sb^{3+} doping of $CsPbI_3$ nanocrystals aiming on improvement of their stability.[14] They found out that the nanocrystal's shape changed towards NPls when ~17% of the B-sites were replaced with Sb^{3+}. While the initial PL QY of the doped NPls was lower than those of pristine nanocrystals, the stability of PL signal was better than that observed for the pristine $CsPbI_3$. The change of morphology at a high Sb^{3+} content was in line with a previous report of Dong et al. who studied the influence of M^{3+} (M = Bi, Al, In) cations on the growth of $CsPbBr_3$ and $CsPbCl_xBr_{3-x}$ NCs.[77] They found that the addition of trivalent metal cations led to the formation of two populations, namely thinner NPls (2.5±0.3 nm) and thicker nanocrystals (thickness ~8.5±0.8 nm). DFT calculations showed that Bi^{3+} ions prefer to bind with (010) crystal facets and constrained further growth in this direction, thus acting as capping ligands for anisotropic growth.

Parveen et al. showed that a progressive increase of the $CeBr_3/TeCl_3$ molar ratio used in solvothermal synthesis of $MAPbBr_3$ led to a decrease of both lateral and vertical dimensions of NPls, which was accompanied by a systematic blue-shift in the absorption and PL band positions and increase of PL QY.[73] They proposed that large amount of dopants may change the reactivity of OlAm or stimulate NPls exfoliation through some kind of intercalation process. Cao et al. showed that trivalent lanthanide doping with Lu^{3+}, $Gd^{3+,}$ or Nd^{3+} cations enlarged the energy barrier for the formation of intermediated 2.5-monolayered $CsPbBr_3$ NPls, thus changing the growth kinetics and offering a possibility to predominantly obtain metastable 2 ML NPls (Figure 3c).[74] Zhou et al. observed that the addition of $EuBr_3$, $SbBr_3$, or $BaBr_2$ into a precursor mixture during the LARP synthesis induced anisotropic growth of square-like 5ML doped $CsPbBr_3$ NPls.[71] They proposed that different mechanisms should be responsible for the anisotropic growth for different dopants: while in the case of Eu^{3+} and Ba^{2+} doping, a suppressed growth in one dimension resulted from the hard/soft − acid/base principle, Sb^{3+} dopant hindered the formation of mixed 5 ML / 6 ML NPls due to the enhanced growth energy barrier. The obtained Sb^{3+}-doped $CsPbBr_3$ NPls possessed short PL lifetime of 1.48 ns, high exciton binding energy of 202 meV, and maintained high PL QY of 95% after three purification cycles.

Gao et al. demonstrated that the progressive addition of $CuCl_2$ into a reaction mixture influenced both the morphology and optical properties of $CsPbCl_3$ NCs.[25] They claimed that the observed change from a cubic to NPl shape should be caused by a high reactivity of Cu^{2+} ions, which competed with OlAm to promote crystal growth. Both Cu^{2+} (as was concluded from the comparison of doping with Cu^{2+}, Eu^{3+}, and Zn^{2+}) and Cl^- ions contributed to elimination of intrinsic and surface defects, which resulted in significant improvement of the PL QY from 3% to 75 % for the doped NPls. Blue LED made from these doped NPLs after partial anion exchange demonstrated high stability of the electroluminescence, which indicates the positive role of Cu^{2+} ion doping in suppressing the ion migration. It is worth noting, however, that it is quite difficult to distinguish between separate contributions of the B-site doping, an increase in the halide environment, and a change in dimension to the observed improvements in optical properties and stability. Song et al. applied treatment with $NiBr_2$ as a passivation strategy to improve the PL efficiency and stability

of $CsPbBr_3$ NPls.[24] An introduction of Ni atoms into a $CsPbBr_3$ lattice was confirmed by X-ray diffraction analysis and X-ray photoelectron spectroscopy. In control experiments, it was shown that the use of Ni^{2+} or Br^- solely gives negligible effect on NPls properties. Ni-Br passivation resulted in the improved stability of the PL signal of doped $CsPbBr_3$ NPls (Figure 3d), which could be attributed to either doping-induced lattice modification or surface passivation of Br^- anion vacancies.

Table 1. Examples of B-site doping of perovskite NPls

Composition	Dopant	Doping strategy	Thickness	Band edge PL peak position, nm	Dopant content*	PL QY*, %	Impact	Ref.
$CsPbCl_3$	Cu^{2+}	In-situ, hot-injection	3 nm	407	–	75	Change of kinetics of the reaction, improved PL QY, reduced trap states density, improved stability of electroluminescence	[25]
$CsPbBr_3$	Bi^{3+}	In-situ, One-pot heating up	2.5 nm, 3ML	458	8.3 % to Pb	–	Change of kinetics of the reaction, improved PL QY,	[77]
$CsPbBr_3$	Lu^{3+}	In-situ, LARP	1.3 nm, 2 ML	431	11.7 mol %	14.8	Control over kinetics of the reaction	[74]
$CsPbBr_3$	Gd^{3+}, Nd^{3+}	In-situ, LARP	2 ML	–	–	–	Control over kinetics of the reaction	[74]
$CsPbBr_3$	Ba^{2+}	In-situ, LARP	5 ML	463	2.6 %	67	Change of kinetics of the reaction	[71]
$CsPbBr_3$	Eu^{3+}	In-situ, LARP	5 ML	463	1.8 %	66	Change of kinetics of the reaction	[71]
$CsPbBr_3$	Sb^{3+}	In-situ, LARP	5 ML	465	3.2 %	95	Change of kinetics of the reaction, shorter PL lifetime, high PL QY	[71]
$CsPbBr_3$	Ni^{2+}	In-situ, LARP	3 nm, 5 ML	454	–	78	Improved PL QY, improved stability of PL	[24]
$CsPbBr_3$	Cd^{2+}	Post-synthetic treatment	2.8 nm, 5 ML	430–465	–	–	Spectral tunability, improved PL QY, enhanced 2PA cross-section	[78]
$MAPbBr_3$	Ce^{3+}	In-situ, solvothermal	7–2 ML	504–454	–	63–100	Change of kinetics of the reaction, increase of recombination rate, increased PL QY	[73]
$MAPbBr_3$	Tb^{3+}	In-situ, solvothermal	down to 2 ML	500–416	1.4 %	60–70	Change of kinetics of the reaction, increase of recombination rate, increased PL QY	[73]
$CsPbI_3$	Sb^{3+}	In-situ, hot-injection	5 nm	684	20 % to Pb	67	Change of kinetics of the reaction, improved stability of PL	[14]

* Optimal dopant content and the highest achieved PL QY are specified if provided in the respective reference

3.2 Post-synthetic doping of NPls

The post-synthetic treatment brings more control over the doping process, and allows us to study its influence on the optoelectronic properties of the perovskite NPls regardless of possible disturbance of the synthetic process. Several approaches for the post-synthetic B-site doping occurring through partial cation exchange have been reported so far. Thorough studied provided information on how doping dynamics depends on precursor choice, solvents, and ligands. In the most cases, metal halide salts dissolved in polar/nonpolar solvents alongside with ligands were used for partial cation exchange. The advantage of this approach is that halide vacancies can additionally be passivated during the treatment, which leads to an increase in the PL QY and an improvement in the stability of perovskite nanostructures. A typical signature of the successful doping is a shift of absorption and PL bands, induced by lattice shrinking or expansion due to different ionic radii of Pb^{2+} and guest cations.[64] In some cases, the shift of PL and absorption bands may not be observed, which means that the added cations may rather be located at the surface.[79,80]

We notice that while a high surface-to-volume ratio of NPls should in principle facilitate post-synthetic doping starting from the surface, brittle nature of ultrathin NPls may be sensitive to the removal of the B-site cations or halides during the exchange reaction.[81] Thus, efforts were made to develop more mild post-synthetic doping protocols. Mir et al.[75] designed a post-synthetic doping strategy based on the treatment of perovskite nanocubes and NPls with Mn^{2+} and Yb^{3+} precursors dissolved in a 3-to-1 mixture of good (toluene)/poor (acetone or methyl acetate) solvents. They showed that a careful choice of solvents and their ratio is important for the successful doping of perovskite nanostructures of different chemical compositions. Wu et al. further proposed a one-step bi-phasic strategy for the post-synthetic doping of $CsPbX_3$ (X = Cl, Br) NPls with Mn^{2+} ions (Figure 4a), which avoided the treatment with antisolvent.[65] NPls were dissolved in hexane, while Mn^{2+} precursor was dissolved in water, so that the doping occurred at the hexane/water interface acting as a semi-permeable membrane. The roles of ligands and Mn^{2+} precursors in this process were individually accessed using a two-step post-synthesis approach (Figure 4b). It was revealed that Mn^{2+} halides facilitated doping by maintaining an appropriate octahedral factor of the perovskite lattice, while OlAm played a role of a molecular shuttle transferring Mn^{2+} ions from water to hexane. Additionally, post-synthetic doping of $CsPbBr_3$ NPls with Cd^{2+} ions in a nonpolar solvent has been recently reported.[78] It was shown that a careful choice of precursors, ligands, and concentrations determined the doping kinetics. The use of Cd-acetate allowed for fine-tuning of the PL peak position at a moderate rate with a little impact on PL QY. Oppositely, the use of the Cd-bromide precursor resulted in a negligible doping, which was accompanied by a strong increase of PL QY due to the passivation of surface trap states. It was shown that the doping rate could be increased by dilution, which can be attributed to the formation of vacant sites which are then available for doping. In this case, a fast doping process could be monitored in situ as a change of absorption and PL bands. A drawback of this approach is the poor stability of the doped NPls. To address this, a two-step doping strategy with Cd-acetate and Cd-bromide precursors was used to insert Cd^{2+} ions inside the NPls and to provide favorable

surface passivation. These results indicate the necessity to consider and adjust multiple parameters for the achievement of successful post-synthetic doping of perovskite NPls.

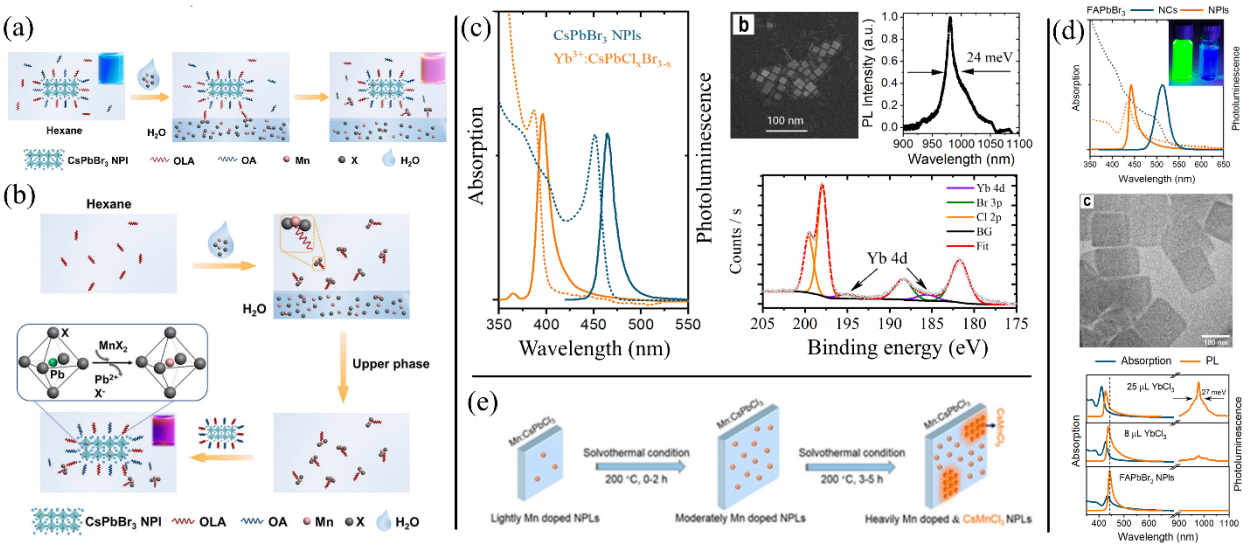

Figure 4. (a) One-step bi-phasic post-synthetic doping $CsPbBr_3$ NPls with Mn^{2+} ions at the hexane/water interface. (b) Two-step post-synthetic doping underlines the pivotal role of OlAm as a molecular shuttle, responsible for MX_2 transport. Reproduced with permission.[65] Copyright 2022, Wiley-VCH. (c) Anion-assisted Yb^{3+}-doping of $CsPbBr_3$ NPls leads to a shift of the band edge emission and the appearance of a new near-infrared PL band related to Yb^{3+} dopants, whose successful insertion was confirmed by XPS. (d) Anion-assisted method can be utilized for room-temperature doping of 2 ML hybrid organic-inorganic $FAPbBr_3$ perovskite NPls with Yb^{3+} ions. Reproduced with permission.[82] Copyright 2023, Royal Society of Chemistry. (e) Two-step Mn^{2+} doping strategy consisting of light doping during the hot-injection synthesis followed by a solvothermal treatment for achieving heavily doped or spinodal decomposed $CsPbCl_3$ NPls. Reproduced with permission.[69] Copyright 2018, American Chemical Society.

Imperfections of the perovskite matrix play an important role in the successful doping. Huang et al. proposed a halide exchange-driven cation exchange mechanism for the post-synthetic doping of $CsPbBr_3$ perovskite nanocrystals with Mn^{2+} ions.[83] By comparison of treatments of $CsPbBr_3$ and $CsPbCl_3$ nanocrystals with $MnCl_2$ and Mn-acetate precursors, they showed that the preceding Br^- to Cl^- anion exchange is the prerequisite for successful cation doping. Zhang et al.[84] further utilized anion-assisted cation doping to produce Mn^{2+}-doped $CsPbCl_xBr_{3-x}$ NPls. $MnCl_2$ precursor was dissolved in N,N- dimethylformamide and added to a solution of $CsPbBr_3$ NPls inducing simultaneous anion exchange and cation doping.

More recently, Tatarinov et al. modified the method of anion-assisted cation doping in a nonpolar solvent to obtain dual-wavelength emitting Yb^{3+}-doped $CsPbCl_3Br_{3-x}$ NPls with an ultra-narrow near-infrared emission band (Figure 4c).[82] $YbCl_3$ and OlAm in toluene were added to $CsPbBr_3$ NPls colloidal solution at room temperature, which induced an anion exchange. During this process, $YbCl_3$ was embedded into the perovskite lattice providing the B-site doping, which

was confirmed by PL and X-ray photoelectron spectroscopy (XPS). This approach allowed to avoid any use of aggressive acids and nonpolar solvents, and thus, it is suitable for doping fragile perovskite nanostructures. As an example, doping 2 ML hybrid organic-inorganic $FAPbBr_3$ perovskite NPls with Yb^{3+} ions using this particular approach has been demonstrated (Figure 4d). Besides, Mn^{2+} doping and Mn^{2+}/Yb^{3+} co-doping (triple-wavelength emitting) of $CsPbCl_3Br_{3-x}$ NPls were realized. Interestingly, doping NPls with Mn^{2+} or Yb^{3+} ions followed different dynamics: Yb^{3+} doping stopped immediately after the anion exchange, while Mn^{2+} doping continued during significant time indicating more feasible insertion and migration of Mn^{2+} ions. Moreover, the formation of additional defects through washing with ethyl acetate facilitated further doping and provided higher PL QY of the near-infrared (NIR) emission from Yb^{3+} dopants. These observations may help for further development of the post-synthetic doping protocols.

Apart from the treatment with metal salts in colloidal solutions, a combined two-step strategy composed of initial in-situ Mn^{2+} doping and post-synthetic solvothermal doping was proposed by Li et al.[69] (Figure 4e). At the first stage, small (lateral sizes and thickness 20 nm and 3 nm, respectively) lightly doped Mn^{2+}:$CsPbCl_3$ perovskite NPls were obtained by hot injection of Cs-oleate into a $PbCl_2$ and $MnCl_2$ precursors. Then, the solution was transferred to an autoclave for further solvothermal reaction. After the solvothermal treatment, the lateral NPls sizes almost doubled while the thickness remained the same, which indicated the oriented attachment of smaller NPls during the second stage. Prolongation of the solvothermal treatment stimulated the insertion of more Mn^{2+} ions into the NPls (heavily doped), which was accompanied by an enhancement of Mn^{2+}-related emission and shifts of the Mn^{2+}-related and band-edge emission peaks positions. More interestingly, at a higher doping ratio, spinodal decomposition induced a formation of a new $CsMnCl_3$ phase without significant change in NPl size or morphology.

3.3 NPls doped with optically active Mn^{2+} and Yb^{3+} ions

3.3.1 Mn^{2+} ions

Doping semiconductor nanostructures with Mn^{2+} ions attracted a lot of attention because this approach allows us to introduce new magnetic and optical properties.[85,86] Dual-band emission from Mn^{2+}-doped semiconductor nanocrystals is attractive for broadband emitters and multicolor imaging, while a large Stoke shift may be useful for solar concentrators. Lead halide perovskites allow for convenient tuning of their bandgaps to precisely engineer the desired dual-band emission properties and to study the mechanism of photoexcitation transfer.[18] Soon after the appearance of pioneering studies on the doping perovskite nanocrystals with Mn^{2+} ions in 2016,[18,19] Mir et al. demonstrated the synthesis of Mn^{2+}-doped $CsPbCl_3$ perovskite NPls with PL QY of 20% under an optimized Mn^{2+} to Pb^{2+} content of 0.8 %.[66] The synthesis was carried out at room temperature under an ambient atmosphere by injecting Pb^{2+}, Mn^{2+}, and Cl^- precursors into a solution containing ODE, Cs-oleate, OA and OlAm ligands. Since then, numerous techniques for both in-situ or post-synthetic doping of perovskite NPls with Mn^{2+} have been developed. Mn^{2+}-precursor to Pb^{2+} feeding ratio, ligands, and reaction conditions should be carefully adjusted to both maintain the

2D geometry and to ensure sufficient Mn^{2+} loading amount aiming for strong orange emission. For instance, Adhikari et al. used alkylamine hydrochloride to control the Mn^{2+} doping of $CsPbCl_3$ nanocrystals.[87] A variation of Cs-to-Pb precursor amount allowed for the tuning of the morphology of the doped nanostructures from nanocubes to NPls. Chen et al. synthesized 4 ML Mn^{2+}-doped $CsPbCl_3$ perovskite NPls by injection of Cs-oleate into a mixture of precursors and ligands at 100 °C under ambient conditions.[68] They studied the influence of injection temperature, time of reaction, and Mn-to-Pb feeding ratio on the morphology of the doped perovskite NPls to optimize their PL QY. Under the optimized synthetic conditions, NPls demonstrated PL QY over 53% and good stability of optical responses upon long-term storage. Besides, tuning the Mn-Pb feed ratio allowed to adjust the emission color from blue-violet to orange-red. Liu et al. used solvothermal synthesis to obtain Mn^{2+}-doped $CsPbCl_3$ perovskite nanostructures of a varied morphology (both nanocubes and NPls), which was achieved by varying amount of ligands.[88] They showed that under the same Mn-to-Pb molar feed ratio, NPls were more heavily doped with Mn^{2+} ions, thus having much brighter Mn^{2+} emission as compared to their cubic counterparts. The thickness control of the doped NPls was achieved by variation of the solvothermal reaction time.

Davis et al. studied the influence of the ratio of long/short ligands on the morphology and optical properties of $CsPbBr_3$ nanocrystals and NPls produced by LARP method.[67] They found out that using a 4-to-1 ratio of long-to-short ligands and {75-80 % acids to 20-25 % amines} was optimal for the formation of the NPls with narrow emission bands and high PL QY. They pointed out that larger number of Mn^{2+} (under the same Mn-to-Pb feeding ratio) became introduced into perovskite NPls when their stoichiometry changed from Cl-rich to Br-rich, which was accompanied by a reduction of ratio of integrated PL intensity of Mn^{2+}-related emission to that of the band-edge emission (Figure 5 a,d). The change in the anion composition was accompanied by the reduction of Mn^{2+}-related PL lifetimes, which may be an evidence of the Mn concentration quenching; additionally, a reduction of the host bandgap may facilitate thermally driven back energy transfer.

As can be seen, increasing the dopant concentration and tuning the band gap both had a limited success in terms of increasing the PL QY of the doped perovskite NPls. Therefore, it is necessary to look for new strategies to further increase the PL efficiency. Song et al. proposed to use of co-doping to change the external crystal field environment aiming at the enhancement of Mn^{2+}-related emission.[89] They analyzed the influence of different cations (Eu^{2+}, Ba^{2+}, In^{3+}, Ce^{3+}, Mg^{2+}, Eu^{3+}, Yb^{3+}, Er^{3+}) on the emission of Mn^{2+} dopant in $CsPbCl_3$ nanocrystals and found that Er^{3+} co-doping provided the highest (~100 times) enhancement of the intensity ratio of the dopant emission to band-edge emission due to the highest crystal field strength. Similarly, Er^{3+}/Mn^{2+} co-doping enhanced the $^4T_1 \rightarrow {}^6A_1$ related emission in $CsPbCl_3$ perovskite NPls as compared to the Mn^{2+}-doped ones. Examples and characteristics of Mn^{2+}-doped perovskite NPls are listed in Table 2.

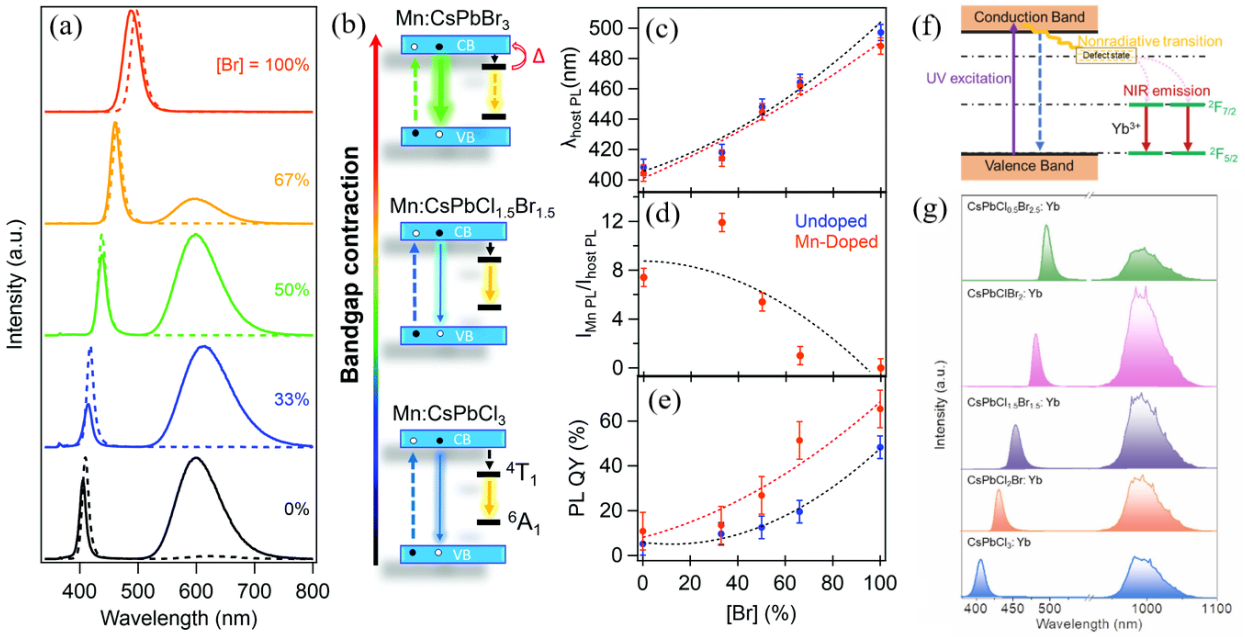

Figure 5. (a) PL spectra of Mn^{2+}-doped (solid lines) and undoped (dashed lines) $CsPbCl_xBr_{3-x}$ NPls with a varied stoichiometry; (b) bandgap contraction of these NPls upon changing the anion composition from Cl^- to Br^-, and (c) corresponding change of the PL peak position of the band-edge related emission. (d) Variation of the anion composition from Cl^- to Br^- induces a gradual reduction of the ratio of integrated PL intensity of Mn^{2+}-related emission to that of the band-edge emission, which may be attributed to Mn concentration quenching or thermally-driven back energy transfer due to the bandgap decrease shown in (b). (e) The overall PL QY of the doped NPls is higher than for the undoped ones, which was attributed to the increase in the tolerance factor and improved structural stability. Reproduced with permission.[67] Copyright 2021, Royal Society of Chemistry. (f) Schematics of the energy relaxation in Yb^{3+}-doped perovskite NPls via simultaneous transfer of photoexcitation to two Yb^{3+} ions, followed by radiative $^2F_{7/2}$-$^2F_{5/2}$ transition in the NIR spectral region. Reproduced with permission.[76] Copyright 2022, Elsevier Ltd. (g) PL spectra of Yb^{3+}-doped $CsPbCl_xBr_{3-x}$ NPls with varied stoichiometry: variation of the anion composition from Cl^- to Br^- in these NPls is accompanied by an increase of the PL QY until the bandgap becomes smaller than a doubled energy of the $^2F_{5/2}$-$^2F_{7/2}$ transition in Yb^{3+} ions.

Table 2. Characteristics of Mn^{2+}- and Yb^{3+}-doped perovskite NPls

Composition	Dopant	Doping strategy	Thickness	Band edge PL peak position, nm	Dopant content*	Band edge PLQY*, %	Dopant PLQY*, %	Total PLQY*, %	Ref
$CsPbCl_3$	Mn^{2+}	Synthesis, injection at room temperature under an ambient atmosphere	2.2 nm, 4 ML	400	0.8 % (to Pb)	0.6	20.3	21	[66]

$CsPbCl_3$	Mn^{2+}	Synthesis, hot-injection in an inert atmosphere	3.0 nm, 5 ML	395	0.2 %	5	2	7	[90]
$CsPbCl_3$	Mn^{2+}	Synthesis, hot-injection in an ambient atmosphere	2.4 nm, 4 ML	400	1.23 % (Mn to {Mn+Pb})	–	–	53.8	[68]
$CsPbCl_3$	Mn^{2+}	Synthesis, LARP	4.8 nm, 7-8 ML	400	0.9 %	–	–	21	[67]
$CsPbCl_3$	Mn^{2+}	Synthesis, Solvothermal	3.0 nm	398	–	–	–	22.2	[88]
$CsPbCl_3$	Mn^{2+}	Post-synthetic, solvothermal	3.0 nm, 5 ML	392	8.8 (mol % to Pb)	–	20.8	–	[69]
$CsPbClBr_2$	Mn^{2+}	Synthesis, LARP	4.8 nm, 7-8 ML	460	–	–	–	50	[67]
$CsPbCl_xBr_{3-x}$	Mn^{2+}	Post-synthetic, anion-assisted cation doping	2.8 nm, 5 ML	400–450	–	–	15.2	40.8	[82]
$CsPbBr_3$	Mn^{2+}	Synthesis, hot-injection	3.0 nm, 5 ML	435	3.2 mol %	–	–	–	[91]
$CsPbBr_3$	Mn^{2+}	Post-synthetic, antisolvent	2.0 nm, 3 ML	440	2.8 %	–	–	–	[75]
$CsPbBr_3$	Mn^{2+}	Post-synthetic, antisolvent	2.4 nm, 4 ML	455	3.2 %	–	–	–	[75]
$CsPbBr_3$	Mn^{2+}	Post-synthetic, antisolvent	3.0 nm, 5 ML	470	4.3 %	–	–	–	[75]
$CsPbBr_3$	Mn^{2+}	Post-synthetic, molecular shuttle	5 ML	461	8 %	–	–	23	[65]
$CsPbBr_3$	Mn^{2+}	Post-synthetic	2.4 nm, 4 ML	460	–	–	–	64.4	[92]
$CsPbBr_3$	Mn^{2+}	Post-synthetic	3.0 nm, 5 ML	465	–	–	–	57	[93]
$CsPbCl_xBr_{3-x}$	Yb^{3+}	Synthesis, hot-injection	6.4 nm	405–480	6.8 mol %	–	–	128 **	[76]
$CsPbCl_xBr_{3-x}$	Yb^{3+}	Post-synthetic, anion-assisted	2.8 nm, 5 ML	385–400	–	–	9.8	–	[82]

		cation doping							
$FAPbCl_xBr_{3-x}$	Yb^{3+}	Post-synthetic, anion-assisted cation doping	2 ML	400–430	–	–	4.2	–	[82]
$CsPbCl_xBr_{3-x}$	$Mn^{2+}+Yb^{3+}$	Post-synthetic, anion-assisted cation doping	2.8 nm, 5 ML	385	–	–	–	–	[82]
$CsPbBr_3$	Yb^{3+}	Post-synthetic, antisolvent	–	–	–	–	–	–	[75]

* Optimal dopant content and the highest achieved PL QY are specified if provided in the respective reference

** PL QY exceeds 100 % because of the quantum-cutting effect (see subsection 3.3.2)

3.3.2 Yb^{3+} ions

Doping perovskite nanocrystals with Yb^{3+} ions has attracted significant attention due to the enormous PL QY achievable via the so-called *quantum-cutting* effect.[20,21] Upon quantum-cutting, the absorption of one high-energy photon (with an energy larger than twice the energy of radiative relaxation) is followed by emission of two low-energy photons. As a consequence, this effect may result in PL QY exceeding 100%. As depicted in Figure 5f, an excitation of a wide bandgap perovskite matrix is followed by simultaneous transfer (most-likely through shallow trap states) of the photoexcitation to two neighboring Yb^{3+} ions, which further emit NIR radiation via $^2F_{7/2} \rightarrow {}^2F_{5/2}$ transition. More details on various quantum-cutting luminescent materials can be found in the review paper by Zhang and Huang.[94] Besides, Yb^{3+}-doping expands the spectral range available for perovskite nanostructures.[95] Since the spectral position of Yb^{3+} emission falls well within the range of Si solar cells' spectral sensitivity, Yb^{3+}-doped perovskite nanostructures are promising for utilization in photovoltaic cells and solar concentrators.[20,96] Very recently, LEDs operating in the near-infrared spectral range based on lanthanide-doped perovskite NCs have been realized.[97–99] Yb^{3+}-doped perovskite nanocrystals have been also proposed as a unique perovskite system that may operate fully in the NIR spectral region using two-photon excitation of perovskite matrix followed by energy transfer to Yb^{3+} dopants.[100] Moreover, Yb^{3+} may be used to stabilize α-phase of $CsPbI_3$ nanocrystals. Shi et al. performed Yb^{3+} doping $CsPbI_3$ perovskite nanocrystals to obtain higher PL QY and better thermal stability; solar cells built with those Yb^{3+} doped $CsPbI_3$ nanocrystals delivered higher power conversion efficiency and improved stability.[15] Thus, the growing popularity of the Yb^{3+} doping calls for the development of new protocols for the Yb^{3+}-doped perovskite nanocrystal's and NPl's fabrication. The examples of Yb^{3+}-doped perovskite NPls are listed in Table 2.

Typical synthetic procedures developed for the doping of perovskite nanocrystals with Yb^{3+} ions require a high temperature of chemical reaction which limits the control over morphology of the resulting products. This limitation could be overcome by post-synthetic doping of the preformed perovskite nanostructures. Yb^{3+}-doped perovskite NPls were first demonstrated by Mir et al.; post-synthetic Mn^{2+} treatment of perovskite nanostructures with various morphologies was extended for Yb^{3+}-doping of $CsPbBr_3$ NPls using $Yb(NO_3)_3$ dissolved in a mixture of methyl acetate and toluene.[75] Anion-assisted post-synthetic Yb^{3+}-doping $CsPbBr_3$ and $FAPbBr_3$ NPls at room temperature has been also reported recently.[82] Interestingly, it was shown that the emission properties of the inserted Yb^{3+} ions depend on their exact position. The PL of dopants located closer to the surface could be quenched by ligands and environment, leading to shorted PL decays and smaller PL QYs. Thermal annealing facilitated migration of the Yb^{3+} ions into the perovskite lattice, and led to improvement of NIR PL QY and prolonged PL decays.

However, it is still challenging to realize a high PL QY of the Yb^{3+}-related NIR emission by post-synthetic NPls doping. One of the possible directions for further development would be to use the concept of co-doping, which has demonstrated its effectiveness in sensitizing the NIR emission from dopant ions in perovskite NCs. In such a co-doped system, one of the dopants acts as a sensitizer for NIR emission from another dopant. In the pioneering work in this field, Zhou et al. demonstrated sensitization of Yb^{3+} ions by Ce^{3+} co-doping, and an overall PL QY reached 146 %.[20] At the same time, Yb^{3+} ions may act as sensitizers for Er^{3+} emission further in the NIR.[22,101,102] Cai et al. suggested possible sensitization of Yb^{3+} ions in the $CsPbCl_3$ perovskite matrix by Mn^{2+} dopants.[103] Zeng et al. demonstrated that co-doping the perovskite nanocrystals with Mn^{2+} and lanthanides is a general strategy to enable intense NIR emission through Mn^{2+}-mediated energy transfer.[104] These studies have shown that co-doping may be considered as a perspective tool for further improvement of lanthanide-doped perovskite NPls. However, Niu et al. have recently shown that Mn^{2+} and Yb^{3+} sensitization in the co-doped nanocrystals is a competitive process, and no sign of Mn^{2+} to Yb^{3+} energy transfer was observed.[105] A similar observation was made by Tatarinov et al. for Mn^{2+}-Yb^{3+} co-doped $CsPbCl_xBr_{3-x}$ NPls.[82] They pointed out that the post-synthetic co-doping using $Mn^{2+}$and Yb^{3+} precursors simultaneously is a competitive process, and different amounts of dopants could be inserted into perovskite host matrix as compared to doping with Mn^{2+}or Yb^{3+} dopants only. This underlines the necessity of careful control over the dopant concentration and thorough experimental and theoretical studies of the processes of energy relaxation in co-doped systems.

Direct synthesis of lanthanide-doped perovskite NPls was reported by Sun et al. who synthesized Yb^{3+}-doped $CsPbX_3$ (X = Cl, Cl/Br) NPls via modified hot-injection method, whose PL spectra are shown in Figure 5g.[76] ODE was replaced with octylamine to dissolve the Cs-precursor, and metal acetates were used instead of metal halides; this allowed to avoid using long-chain OlAm and promoted anisotropic growth of the NPls. Lateral sizes of the NPls were tuned by adjusting the amount of octylamine. Using anion exchange reactions, the authors studied the dependence of PL QY on the NPls stoichiometry and the bandgap. PL QY reached 128 % for the $CsPbClBr_2$ stoichiometry whose bandgap corresponded well twice the energy of $^2F_{5/2}$-$^2F_{7/2}$ Yb^{3+} transition, due to the quantum-cutting effect. Further anion exchange led to a sharp decrease in PL

QY, because the bandgap became smaller than twice the energy of the $^2F_{5/2}$-$^2F_{7/2}$ Yb^{3+} transition which made quantum-cutting impossible. A further development of the thickness control over the NPls synthesis is required to finely tune the bandgap of the perovskite host, thus avoiding the necessity of partial anion exchange, which eventually eliminates the additional treatment steps and possible problems with halide segregation.

4 Applications of perovskite NPls and doping

The attractive properties of perovskite NPls paved the way for their potential applications in LEDs and photodetectors,[106,107] photocatalysis, and nonlinear optics, as illustrated in Figure 6. Large absorption coefficient of perovskite NPls and their long charge carrier diffusion lengths have been utilized in highly efficient photodetectors, including flexible[108] and polarization-sensitive[46] devices. Parveen et al. have recently shown that Eu^{3+} doping of $MAPbBr_3$ NPls used in photodetectors brings numerous improvements in the device performance, namely, higher responsivity and detectivity, faster photoresponse, and enhanced operational stability.[26] Ultrathin nature of NPls facilitates the charge transfer of charge carriers to the surface and may provide more active sites, which is also beneficial for photocatalysis.[109] Indeed, Liu et al. recently showed that the lead-free Cs_2AgBiX_6 NPls demonstrate better photocatalytic CO_2 reduction as compared to their 3D nanocube-shaped counterparts.[110] Also in this field, Wu et al. demonstrated promising performance of $Cs_3Sb_2(Br_xI_{1-x})_9$ NPls for the CO_2 reduction at gas–solid interface.[111] At the same time, metal doping is a promising tool to further optimize the photocatalytic properties of metal-halide perovskites, as has been recently reviewed by Zhong et al.[112] Regarding the NPls, the Mn^{2+} doping of $CsPbBr_3$ NPls was demonstrated to be an efficient tool to boost the photocatalytic CO_2 reduction efficiency.[91]

Ultra-narrow emission from perovskite NPls with Br^- and I^- anions is thickness-tunable across the visible spectral range. Besides, 2D confined NPls possess giant oscillator strength and high radiative recombination rates. For these reasons, both organic-inorganic and fully inorganic perovskite NPls have been actively applied as an active layer in LEDs,[57,113] and exploited in miniature one- or multi-photon excited lasers.[27,114] To obtain high-quality full-color displays, superior emitters in blue, green, and red spectral ranges are required. However, the efficiencies of perovskite-based pure-blue and pure-red LEDs still lag behind those demonstrated for the green spectral range.[115,116] Mixed-halide or strongly-confined perovskite nanocrystals could be used to achieve pure-blue emission, but at a price of poorer stability induced by halide segregation and non-negligible size distribution, respectively. Alternatively, color-pure narrow-emitting blue and red LEDs can be produced using highly monodisperse NPls as an active layer. In this regard, B-site doping of NPls may provide additional improvement in their phase stability, emission characteristics, and charge carrier transport. Moreover, doping perovskite NPls with optically active ions, such as Mn^{2+} and Yb^{3+}, opens the way for construction of orange-, white-, and NIR-emitting LEDs and down-converters. However, several challenges such as NPls merging and Auger recombination-induced efficiency roll-off should be overcome to further increase the efficiency and stability of NPls-based LEDs.[3]

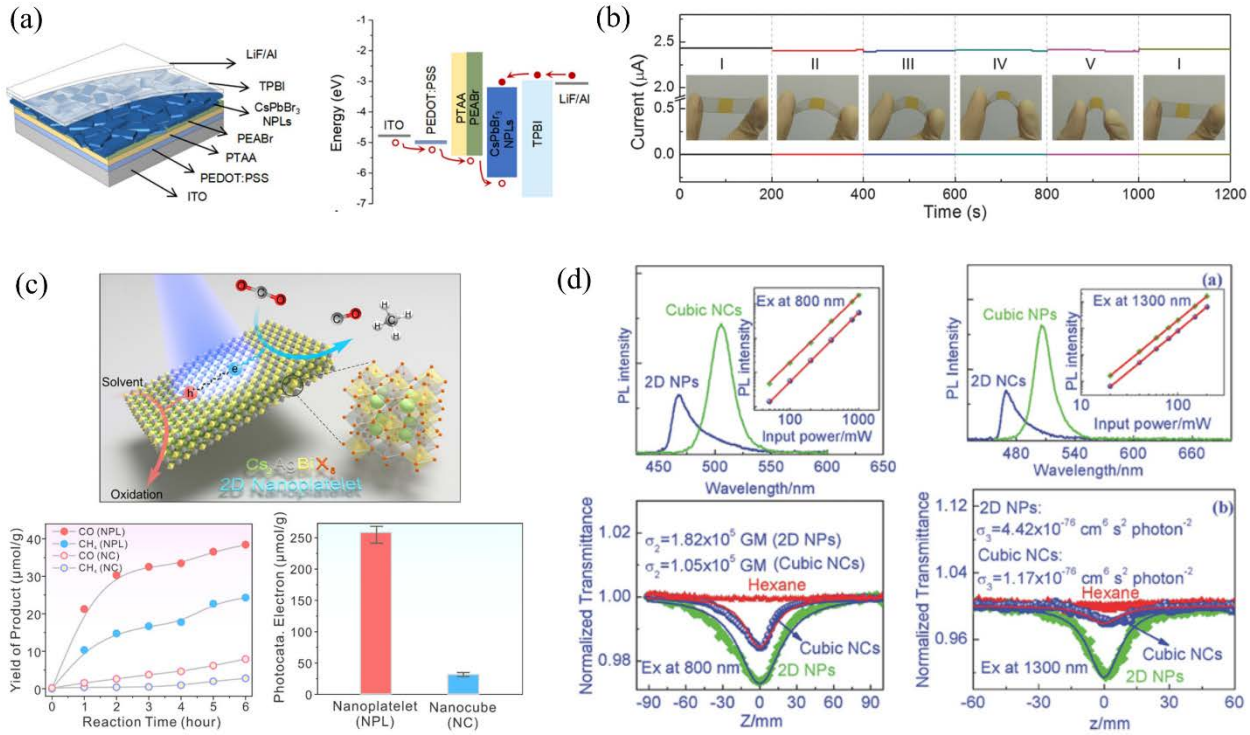

Figure 6. Selected illustration of the application of perovskite NPls in LEDs, photodetectors, photocatalysis, and nonlinear optics. (a) Device structure and its energy diagram for a blue (463 nm) perovskite LED utilizing $CsPbBr_3$ NPls as an active layer. Reproduced with permission.[117] Copyright 2022, American Chemical Society. (b) Electrical stability test at various bending curvatures for a flexible 2D perovskite photodetector. Reproduced with permission.[108] Copyright 2016, Wiley-VCH. (c) $Cs_2AgBiBr_6$ double perovskites demonstrate superior photocatalyzed CO_2 reduction efficiency in their 2D form as compared to their nanocube counterparts. Reproduced with permission.[110] Copyright 2021, American Chemical Society. (d) $CsPbBr_3$ NPls possess enlarged absolute and volume-normalized values of two- and three-photon absorption cross-sections, which renders them attractive for nonlinear optical applications. Reproduced with permission.[118] Copyright 2018, Wiley-VCH.

Metal halide perovskites have also been considered to be perspective nonlinear optical materials.[119–121] Specifically, 2D perovskite NPls demonstrated superior nonlinear optical properties because their 2D form enhances nonlinear optical response due to the 1D quantum confinement. It has been reported that $CsPbBr_3$[118] and $CsPbBr_{2.7}I_{0.3}$[122] NPls possess higher volume-normalized multiphoton absorption cross-section compared to their 3D counterparts, attributed to stronger quantum confinement. Therefore, 2D perovskite NPls are promising materials for numerous nonlinear optical applications such as high-resolution bioimaging, up-converting lasing, optical limiting, etc.[114,123] B-site doping has been considered as an effective tool for further improvement of the nonlinear optical properties of perovskite nanomaterials due to the enhanced coupling between the charge carriers in perovskite matrix with dopant electrons and increased density of the sub-band states.[114,123–126] However, more theoretical and

experimental analysis is required for the generalization of the role of B-site cation doping on nonlinear optical responses from perovskite nanocrystals and NPls.

At the beginning, Ketavath et al. studied the influence of Ni^{2+} doping on the nonlinear optical responses from $CsPbBr_3$ NPls using Z-scan technique,[70] showing that optimized Ni^{2+} content provided enhancement of both two-photon absorption and nonlinear refraction (self-focusing), which was revealed using open-aperture and close-aperture measurements, respectively (Figure 7a,b). Skurlov et al. studied the influence of Cd^{2+} doping on the two-photon absorption cross-section of $CsPbBr_3$ NPls using two-photon absorption-induced PL measurements (Figure 7c).[78] The post-synthetic treatment of the NPls allowed for finely tuning the doping ratio, which could be precisely monitored through a shift of the PL peak position. It was demonstrated that even a small fraction of inserted Cd^{2+} ions induced a strong increase in the third-order nonlinear optical responses of perovskite NPls (Figure 7d). Higher degree of doping induced a gradual decrease of the two-photon absorption cross-section, which was attributed to the structural deterioration of NPl's crystal structure.

He et al. studied nonlinear optical properties of Mn^{2+}-doped $CsPbCl_3$ NPls using Z-scan and PL measurements ($^6A_1 \rightarrow {}^4T_1$ Mn^{2+} emission) under multiphoton (two- and three-photon) excitation.[90] Volume-normalized two- and three-absorption cross-sections enlarged from 183 to 1237 GM/nm^3 (where GM is 10^{-50} cm^4·s·photon^{-1}) and from 3.1×10^{-79} to 2.24×10^{-78} cm^6·s^2·photon^{-2}/nm^3, respectively, when the dimensionality of perovskite nanocrystals reduced from 3D to 2D. Comparison of the linear absorption spectrum with a wavelength dependence of two-photon absorption cross sections suggested 2D confinement-related enhancement of the nonlinear response. This was in good agreement with the enhanced nonlinear optical response from the undoped NPls as compared to their 3D counterparts as reported in Refs.[118,122]

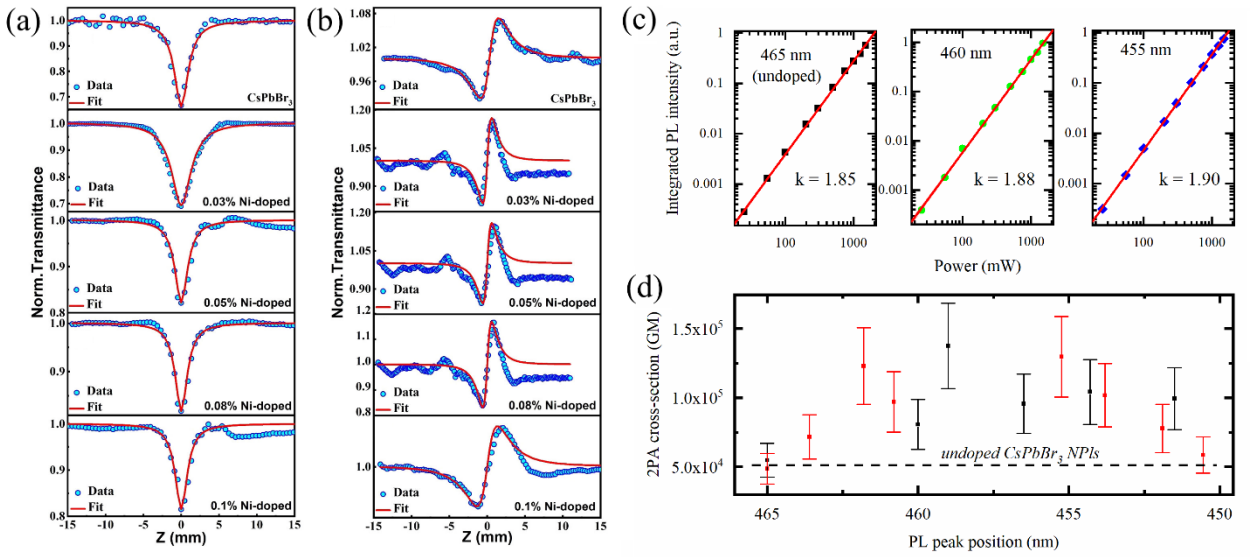

Figure 7. (a) Open-aperture and (b) closed-aperture measurements of the nonlinear absorption and refraction, respectively, in Ni^{2+}-doped $CsPbBr_3$ perovskite NPls with different amounts of dopant. Using 0.08% Ni^{2+}-doping led to two-photon absorption cross-section $\sigma = 4.11\times10^4$ (GM) and nonlinear refraction index $n_2 = 8.4\times10^{-12}$ (cm^2/W). Reproduced with permission.[70] Copyright

2019, American Chemical Society. (c) Dependencies of integrated PL intensities vs excitation power for $CsPbBr_3$ and Cd^{2+}-doped $CsPbBr_3$ NPls with the slopes indicating two-photon excitation. (d) Dependence of the two-photon absorption cross-section of Cd^{2+}-doped $CsPbBr_3$ NPls on their PL peak position, which reflects the level of doping. Reproduced under CC BY license.[78]

Conclusions and outlook

Doping of perovskite NPls on the B-site cation constitutes an active area of contemporary research. Based on the analysis of the respective literature as demonstrated in this review, several key approaches and issues can be underlined:

Doping methods. Introducing the additives during the synthesis can not only modify the optoelectronic properties of the formed NPls but may facilitate their formation and influence the growth. Thus, deeper understanding of the specific role of dopants on the NPls growth and resulting morphology is required. Moreover, metal halides were widely used to produce doped perovskite NPls or nanocrystals. The halide-rich environment during synthesis may mask the effect of doping itself. Hence, more comparative studies using halides, carboxylates, and oleates are required to better recognize the influence of cation doping on the reaction kinetics and physical properties of perovskite NPls.

Physical properties. Combination of further experimental and theoretical studies on how the B-site dopants influence the linear and nonlinear optical and electronic properties of perovskite NPls is of great importance. For instance, it has been recently shown that change in the local periodicity of perovskite lattice upon doping can significantly influence their electronic structure.[127] Further developments in this direction in respect to ultrathin NPls can promote engineering of improved perovskite nanomaterials. A strong influence of the B-site doping on nonlinear optical properties of perovskite NPls has been demonstrated and requires further systematical studies. Being a tool for a better controllable doping, post-synthetic treatment is a useful approach for the experimental studies of dopant-induced changes of NPl properties. Universal and gentle post-synthetic doping methods that have appeared recently open up wide opportunities for studying the changes in physical properties of perovskites upon introduction of various dopants.

Sensitization of optically active ions. Understanding the underlying photophysical processes in perovskite nanocrystals and NPls doped with optically active ions (Mn^{2+}, Yb^{3+}, etc.) is another important research direction. Mechanisms of sensitization of the emissive dopants in perovskite hosts are still under debate, and despite much work has been done to study them in Mn^{2+} and Yb^{3+}-doped perovskite nanocrystals,[18,19,21,100,105,128–132] the generalized models describing dependencies of optical properties of such doped perovskite nanostructures on bandgap, dopant level, temperature, and excitation are in demand. In particular, the concentration dependencies of the optical parameters of doped NPls require further clarification, as they are essential for development of optimized emitters for different applications. Obvious difficulties in determination of the low levels and changes in dopant amount, and various notations used for the percentage of

doping (overall percentage, percentage to B site, percentage to Pb atoms) complicate the analysis of experimental results. Generalization of larger amount of experimental data with the help of machine learning algorithms,[133–135] is likely to provide further progress in this direction.

Co-doping. The concept of co-doping has been rather successful for perovskite nanocrystals in general, but its potential is far from being fully exploited. For instance, introducing additional Ce^{3+}, Mn^{2+}, Cr^{3+}, or Yb^{3+} dopants [20,22,136][137] showed much promise for sensitization of NIR emission from perovskite nanocrystals, but has not been demonstrated for perovskite NPls yet. Thus, further experimental and theoretical study of the processes of energy relaxation in nanostructures with multiple emitting centers is required. Besides, a co-doping strategy may be considered as a tool to enhance the long-term stability of rather fragile perovskite NPls. Recently, Pansa-Ngat et al. showed how incorporation of modest quantities of two divalent cations stabilized $CsPbI_3$ perovskite films.[138] Further research in this direction may pave the way for fabrication of efficient and stable optoelectronic devices based on perovskite NPls.

Acknowledgments

The authors acknowledge financial support from the National Key Research and Development Program of China (project 2022YFE0200200), National Natural Science Foundation of China (52072141, 51972136, 52102170), Postdoctoral Science Foundation of China (2021T140251), the Research Grant Council of Hong Kong SAR (CityU 11317322), and the Croucher Foundation of Hong Kong.

Conflict of interest

The authors declare no conflict of interest.

Author biographies

Aleksandr P. Litvin received his PhD in Optics in 2015 from ITMO University (St. Petersburg, Russia). From 2020 to 2022 he headed the Laboratory “Optics of Quantum Nanostructures” at the same university. He is currently a postdoctoral researcher at the College of Materials Science and Engineering of Jilin University, China. His scientific interests are in optical spectroscopy of near-infrared emitting nanostructures, including quantum dots, nanoplatelets, and perovskites, energy and charge transfer phenomena between nanoparticles, and their utilization in optoelectronic devices.

Andrey L. Rogach received his PhD in Chemistry in 1995 from the Belarusian State University in Minsk, and completed his Habilitation in Experimental Physics at the University of Munich, Germany in 2009. He is currently Yeung Kin Man Chair Professor in Photonics Materials and Founding Director of the Centre for Functional Photonics at City University of Hong Kong. His research focuses on the synthesis, assembly and optical spectroscopy of semiconductor and metal nanocrystals, and their use for optoelectronic applications.

References

[1] M. C. Weidman, A. J. Goodman, W. A. Tisdale, *Chem. Mater.* **2017**, *29*, 5019.

[2] A. Dey, J. Ye, A. De, E. Debroye, S. K. Ha, E. Bladt, A. S. Kshirsagar, Z. Wang, J. Yin, Y. Wang, L. N. Quan, F. Yan, M. Gao, X. Li, J. Shamsi, T. Debnath, M. Cao, M. A. Scheel, S. Kumar, J. A. Steele, M. Gerhard, L. Chouhan, K. Xu, X. Wu, Y. Li, Y. Zhang, A. Dutta, C. Han, I. Vincon, A. L. Rogach, A. Nag, A. Samanta, B. A. Korgel, C.-J. Shih, D. R. Gamelin, D. H. Son, H. Zeng, H. Zhong, H. Sun, H. V. Demir, I. G. Scheblykin, I. Mora-Seró, J. K. Stolarczyk, J. Z. Zhang, J. Feldmann, J. Hofkens, J. M. Luther, J. Pérez-Prieto, L. Li, L. Manna, M. I. Bodnarchuk, M. V. Kovalenko, M. B. J. Roeffaers, N. Pradhan, O. F. Mohammed, O. M. Bakr, P. Yang, P. Müller-Buschbaum, P. V. Kamat, Q. Bao, Q. Zhang, R. Krahne, R. E. Galian, S. D. Stranks, S. Bals, V. Biju, W. A. Tisdale, Y. Yan, R. L. Z. Hoye, L. Polavarapu, *ACS Nano* **2021**, *15*, 10775.

[3] C. Otero-Martínez, J. Ye, J. Sung, I. Pastoriza-Santos, J. Pérez-Juste, Z. Xia, A. Rao, R. L. Z. Hoye, L. Polavarapu, *Adv. Mater.* **2022**, *34*, 1.

[4] Y. Bekenstein, B. A. Koscher, S. W. Eaton, P. Yang, A. P. Alivisatos, *J. Am. Chem. Soc.* **2015**, *137*, 16008.

[5] J. A. Sichert, Y. Tong, N. Mutz, M. Vollmer, S. Fischer, K. Z. Milowska, R. García Cortadella, B. Nickel, C. Cardenas-Daw, J. K. Stolarczyk, A. S. Urban, J. Feldmann, *Nano Lett.* **2015**, *15*, 6521.

[6] F. Liu, C. Ding, Y. Zhang, T. S. Ripolles, T. Kamisaka, T. Toyoda, S. Hayase, T. Minemoto, K. Yoshino, S. Dai, M. Yanagida, H. Noguchi, Q. Shen, *J. Am. Chem. Soc.* **2017**, *139*, 16708.

[7] T. C. Jellicoe, J. M. Richter, H. F. J. Glass, M. Tabachnyk, R. Brady, S. E. Dutton, A. Rao, R. H. Friend, D. Credgington, N. C. Greenham, M. L. Böhm, *J. Am. Chem. Soc.* **2016**, *138*, 2941.

[8] X. Zhang, W. Cao, W. Wang, B. Xu, S. Liu, H. Dai, S. Chen, K. Wang, X. W. Sun, *Nano Energy* **2016**, *30*, 511.

[9] M. Lu, X. Zhang, Y. Zhang, J. Guo, X. Shen, W. W. Yu, A. L. Rogach, *Adv. Mater.* **2018**, *30*, 1804691.

[10] J. Yao, J. Ge, K. Wang, G. Zhang, B. Zhu, C. Chen, Q. Zhang, Y. Luo, S. Yu, H. Yao, **2019**, DOI: 10.1021/jacs.8b11447.

[11] R. K. Behera, A. Dutta, D. Ghosh, S. Bera, S. Bhattacharyya, N. Pradhan, *J. Phys. Chem. Lett.* **2019**, *10*, 7916.

[12] W. Shen, J. Zhang, R. Dong, Y. Chen, L. Yang, S. Chen, Z. Su, Y. Dai, K. Cao, L. Liu, S. Chen, W. Huang, *Research* **2021**, *2021*, DOI: 10.34133/2021/9829374.

[13] X. Shen, Y. Zhang, S. V. Kershaw, T. Li, C. Wang, X. Zhang, W. Wang, D. Li, Y. Wang, M. Lu, L. Zhang, C. Sun, D. Zhao, G. Qin, X. Bai, W. W. Yu, A. L. Rogach, *Nano Lett.* **2019**, *19*, 1552.

[14] S. Bera, D. Ghosh, A. Dutta, S. Bhattacharyya, S. Chakraborty, N. Pradhan, *ACS Energy Lett.* **2019**, *4*, 1364.

[15] J. Shi, F. Li, J. Yuan, X. Ling, S. Zhou, Y. Qian, W. Ma, *J. Mater. Chem. A* **2019**, *7*, 20936.

[16] C. M. Guvenc, Y. Yalcinkaya, S. Ozen, H. Sahin, M. M. Demir, *J. Phys. Chem. C* **2019**,

123, 24865.

[17] W. Xia, Z. Ren, Z. Zheng, C. Luo, J. Li, W. Ma, X. Zhou, Y. Chen, *Nanoscale* **2023**, *15*, 1109.

[18] W. Liu, Q. Lin, H. Li, K. Wu, I. Robel, J. M. Pietryga, V. I. Klimov, *J. Am. Chem. Soc.* **2016**, *138*, 14954.

[19] D. Parobek, B. J. Roman, Y. Dong, H. Jin, E. Lee, M. Sheldon, D. H. Son, *Nano Lett.* **2016**, *16*, 7376.

[20] D. Zhou, D. Liu, G. Pan, X. Chen, D. Li, W. Xu, X. Bai, H. Song, *Adv. Mater.* **2017**, *29*, 1704149.

[21] T. J. Milstein, D. M. Kroupa, D. R. Gamelin, *Nano Lett.* **2018**, *18*, 3792.

[22] X. X. Zhang, Y. Zhang, X. X. Zhang, W. Yin, Y. Wang, H. Wang, M. Lu, Z. Li, Z. Gu, W. W. Yu, *J. Mater. Chem. C* **2018**, *6*, 10101.

[23] W. Lee, S. Hong, S. Kim, *J. Phys. Chem. C* **2019**, *123*, 2665.

[24] J. Song, Y. Gao, Z. Meng, Z. Jiang, X. Cao, Q. Zeng, T. Hu, *Opt. Mater. (Amst).* **2023**, *138*, 113611.

[25] Y. Gao, C. Luo, C. Yan, W. Li, C. Liu, W. Yang, *J. Colloid Interface Sci.* **2022**, *607*, 1796.

[26] S. Parveen, M. Das, S. Ghosh, P. K. Giri, *Nanoscale* **2022**, 6402.

[27] T. Song, Q. X. Ma, Q. Wang, H. L. Zhang, *Mater. Adv.* **2022**, *3*, 756.

[28] S. Das Adhikari, N. Pradhan, *Front. Mater.* **2020**, *7*, 1.

[29] S. Parveen, P. K. Giri, *Nanoscale Adv.* **2022**, *4*, 995.

[30] Y.-T. Li, L. Han, H. Liu, K. Sun, D. Luo, X.-L. Guo, D.-L. Yu, T.-L. Ren, *ACS Appl. Electron. Mater.* **2022**, *4*, 547.

[31] F. Zhang, H. Zhong, C. Chen, X. G. Wu, X. Hu, H. Huang, J. Han, B. Zou, Y. Dong, *ACS Nano* **2015**, *9*, 4533.

[32] L. Protesescu, S. Yakunin, M. I. Bodnarchuk, F. Krieg, R. Caputo, C. H. Hendon, R. X. Yang, A. Walsh, M. V. Kovalenko, *Nano Lett.* **2015**, *15*, 3692.

[33] P. Tyagi, S. M. Arveson, W. A. Tisdale, *J. Phys. Chem. Lett.* **2015**, *6*, 1911.

[34] Q. A. Akkerman, S. G. Motti, A. R. Srimath Kandada, E. Mosconi, V. D'Innocenzo, G. Bertoni, S. Marras, B. A. Kamino, L. Miranda, F. De Angelis, A. Petrozza, M. Prato, L. Manna, *J. Am. Chem. Soc.* **2016**, *138*, 1010.

[35] I. Levchuk, P. Herre, M. Brandl, A. Osvet, R. Hock, W. Peukert, P. Schweizer, E. Spiecker, M. Batentschuk, C. J. Brabec, *Chem. Commun.* **2017**, *53*, 244.

[36] I. Levchuk, A. Osvet, X. Tang, M. Brandl, J. D. Perea, F. Hoegl, G. J. Matt, R. Hock, M. Batentschuk, C. J. Brabec, *Nano Lett.* **2017**, *17*, 2765.

[37] H. Zheng, W. Pan, W. Shen, *Nanotechnology* **2018**, *29*, 455601.

[38] B. J. Bohn, Y. Tong, M. Gramlich, M. L. Lai, M. Döblinger, K. Wang, R. L. Z. Hoye, P. Müller-Buschbaum, S. D. Stranks, A. S. Urban, L. Polavarapu, J. Feldmann, *Nano Lett.* **2018**, *18*, 5231.

[39] H. Huang, Y. Li, Y. Tong, E. Yao, M. W. Feil, A. F. Richter, M. Döblinger, A. L. Rogach, J. Feldmann, L. Polavarapu, *Angew. Chemie Int. Ed.* **2019**, *58*, 16558.

[40] H. Fang, W. Deng, X. Zhang, X. Xu, M. Zhang, J. Jie, X. Zhang, *Nano Res.* **2019**, *12*, 171.

[41] X. Liu, Z. Luo, W. Yin, A. P. Litvin, A. V. Baranov, J. Zhang, W. Liu, X. Zhang, W. Zheng, *Nanoscale Adv.* **2020**, *2*, 1973.

[42] O. Vybornyi, S. Yakunin, M. V. Kovalenko, *Nanoscale* **2016**, *8*, 6278.

[43] G. Almeida, L. Goldoni, Q. Akkerman, Z. Dang, A. H. Khan, S. Marras, I. Moreels, L. Manna, *ACS Nano* **2018**, *12*, 1704.

[44] A. Pan, B. He, X. Fan, Z. Liu, J. J. Urban, A. P. Alivisatos, L. He, Y. Liu, *ACS Nano* **2016**, *10*, 7943.

[45] J. Shamsi, Z. Dang, P. Bianchini, C. Canale, F. Di Stasio, R. Brescia, M. Prato, L. Manna, *J. Am. Chem. Soc.* **2016**, *138*, 7240.

[46] X. Sheng, G. Chen, C. Wang, W. Wang, J. Hui, Q. Zhang, K. Yu, W. Wei, M. Yi, M. Zhang, Y. Deng, P. Wang, X. Xu, Z. Dai, J. Bao, X. Wang, *Adv. Funct. Mater.* **2018**, *28*, 1800283.

[47] W. Zhai, J. Lin, Q. Li, K. Zheng, Y. Huang, Y. Yao, X. He, L. Li, C. Yu, C. Liu, Y. Fang, Z. Liu, C. Tang, *Chem. Mater.* **2018**, *30*, 3714.

[48] Q. Pan, H. Hu, Y. Zou, M. Chen, L. Wu, D. Yang, X. Yuan, J. Fan, B. Sun, Q. Zhang, *J. Mater. Chem. C* **2017**, *5*, 10947.

[49] Y. Tong, E. Bladt, M. F. Aygüler, A. Manzi, K. Z. Milowska, V. A. Hintermayr, P. Docampo, S. Bals, A. S. Urban, L. Polavarapu, J. Feldmann, *Angew. Chemie - Int. Ed.* **2016**, *55*, 13887.

[50] C. Otero-Martínez, D. García-Lojo, I. Pastoriza-Santos, J. Pérez-Juste, L. Polavarapu, *Angew. Chemie Int. Ed.* **2021**, *60*, 26677.

[51] M. Chen, Y. Zou, L. Wu, Q. Pan, D. Yang, H. Hu, Y. Tan, Q. Zhong, Y. Xu, H. Liu, B. Sun, Q. Zhang, *Adv. Funct. Mater.* **2017**, *27*, 1701121.

[52] M. Chen, H. Hu, N. Yao, X. Yuan, Q. Zhong, M. Cao, Y. Xu, Q. Zhang, *J. Mater. Chem. C* **2019**, *7*, 14493.

[53] D. Zhang, M. Yu, Y. Xu, D. Li, Y. Huang, C. Yu, C. Tang, J. Lin, *Opt. Mater.* **2022**, *127*, 112257.

[54] C. Xie, A. Zhang, L. Chen, P. Yang, *ACS Appl. Nano Mater.* **2022**, *5*, 12552.

[55] S. Parveen, K. K. Paul, P. K. Giri, *ACS Appl. Mater. Interfaces* **2020**, *12*, 6283.

[56] V. A. Hintermayr, A. F. Richter, F. Ehrat, M. Döblinger, W. Vanderlinden, J. A. Sichert, Y. Tong, L. Polavarapu, J. Feldmann, A. S. Urban, V. A. Hintermayr, A. F. Richter, F. Ehrat, J. A. Sichert, Y. Tong, L. Polavarapu, J. Feldmann, A. S. Urban, M. Döblinger, W. Vanderlinden, *Adv. Mater.* **2016**, *28*, 9478.

[57] D. Yang, Y. Zou, P. Li, Q. Liu, L. Wu, H. Hu, Y. Xu, B. Sun, Q. Zhang, S. Lee, *Nano Energy* **2018**, *47*, 235.

[58] J. Shamsi, P. Rastogi, V. Caligiuri, A. L. Abdelhady, D. Spirito, L. Manna, R. Krahne, *ACS Nano* **2017**, *11*, 10206.

[59] J. Shamsi, D. Kubicki, M. Anaya, Y. Liu, K. Ji, K. Frohna, C. P. Grey, R. H. Friend, S. D. Stranks, *ACS Energy Lett.* **2020**, *5*, 1900.

[60] Y. Ding, T. Li, X. Li, E. A. Tsiwah, C. Liu, P. Gao, T. Zeng, Y. Chen, X. Zhao, Y. Xie, *CrystEngComm* **2019**, *21*, 2388.

[61] M. A. Uddin, J. D. Glover, S. M. Park, J. T. Pham, K. R. Graham, *Chem. Mater.* **2020**, *32*, 5217.

[62] J. K. Chen, J. P. Ma, S. Q. Guo, Y. M. Chen, Q. Zhao, B. Bin Zhang, Z. Y. Li, Y. Zhou, J. Hou, Y. Kuroiwa, C. Moriyoshi, O. M. Bakr, J. Zhang, H. T. Sun, *Chem. Mater.* **2019**, *31*, 3974.

[63] H. Huang, R. Li, S. Jin, Z. Li, P. Huang, J. Hong, S. Du, W. Zheng, X. Chen, D. Chen, *ACS Appl. Mater. Interfaces* **2021**, *13*, 34561.

[64] W. van der Stam, J. J. Geuchies, T. Altantzis, K. H. W. van den Bos, J. D. Meeldijk, S. Van Aert, S. Bals, D. Vanmaekelbergh, C. de Mello Donega, *J. Am. Chem. Soc.* **2017**, *139*, 4087.

[65] L. Wu, Y. Wang, M. Kurashvili, A. Dey, M. Cao, M. Döblinger, Q. Zhang, J. Feldmann, H. Huang, T. Debnath, *Angew. Chemie Int. Ed.* **2022**, *61*, e202115852.

[66] W. J. Mir, M. Jagadeeswararao, S. Das, A. Nag, *ACS Energy Lett.* **2017**, *2*, 537.

[67] A. H. Davis, S. Li, H. Lin, C. Chu, J. M. Franck, G. Leem, M. M. Maye, W. Zheng, *J. Mater. Chem. C* **2021**, *9*, 14226.

[68] Z. Chen, L. Dong, C. Zhou, B. Zhou, Z. Zheng, R. Chen, J. Zang, *CrystEngComm* **2021**, *23*, 793.

[69] Z. J. Li, E. Hofman, A. H. Davis, A. Khammang, J. T. Wright, B. Dzikovski, R. W. Meulenberg, W. Zheng, *Chem. Mater.* **2018**, *30*, 6400.

[70] R. Ketavath, N. K. Katturi, S. G. Ghugal, H. K. Kolli, T. Swetha, V. R. Soma, B. Murali, *J. Phys. Chem. Lett.* **2019**, *10*, 5577.

[71] A. Zhou, Y. Xie, F. Wang, R. Liang, Q. Ou, S. Zhang, *J. Phys. Chem. Lett.* **2022**, *13*, 4634.

[72] L. G. Bonato, R. F. Moral, G. Nagamine, A. Alo, J. C. Germino, D. S. da Silva, D. B. Almeida, L. F. Zagonel, F. Galembeck, L. A. Padilha, A. F. Nogueira, *Angew. Chemie - Int. Ed.* **2020**, *59*, 11501.

[73] S. Parveen, P. K. Prasanna, S. Chakraborty, P. K. Giri, *J. Mater. Chem. C* **2021**, *9*, 2437.

[74] Q. Cao, A. Ilyas, S. Zhang, Z. Ju, F. Sun, T. Liu, Y. Yang, Y. Lu, X. Liu, R. Deng, *Nanoscale* **2021**, *13*, 11552.

[75] W. J. Mir, Y. Mahor, A. Lohar, M. Jagadeeswararao, S. Das, S. Mahamuni, A. Nag, *Chem. Mater.* **2018**, *30*, 8170.

[76] R. Sun, D. Zhou, P. Lu, X. Jing, X. Zhuang, S. Liu, Y. Wang, X. Bai, W. Xu, H. Song, *Nano Energy* **2022**, *93*, 106815.

[77] X. Dong, E. Acheampong Tsiwah, T. Li, J. Hu, Z. Li, Y. Ding, Z. Deng, W. Chen, L. Xu, P. Gao, X. Zhao, Y. Xie, *Nanoscale* **2019**, *11*, 7903.

[78] I. D. Skurlov, A. V. Sokolova, D. A. Tatarinov, P. S. Parfenov, D. A. Kurshanov, A. O. Ismagilov, A. V. Koroleva, D. V. Danilov, E. V. Zhizhin, S. V. Mikushev, A. N. Tcypkin,

A. V. Fedorov, A. P. Litvin, *Materials.* **2022**, *15*, 7676.

[79] F. Li, Y. Liu, H. Wang, Q. Zhan, Q. Liu, Z. Xia, *Chem. Mater.* **2018**, *30*, 8546.

[80] N. Mondal, A. De, A. Samanta, *ACS Energy Lett.* **2019**, *4*, 32.

[81] Z. Yang, M. Wei, O. Voznyy, P. Todorovic, M. Liu, R. Quintero-Bermudez, P. Chen, J. Z. Fan, A. H. Proppe, L. N. Quan, G. Walters, H. Tan, J. W. Chang, U. S. Jeng, S. O. Kelley, E. H. Sargent, *J. Am. Chem. Soc.* **2020**, *141*, 8296.

[82] D. A. Tatarinov, A. V Sokolova, I. D. Skurlov, D. V. Danilov, A. V. Koroleva, N. K. Kuzmenko, Y. A. Timkina, M. A. Baranov, E. V. Zhizhin, A. N. Tcypkin, A. P. Litvin, *J. Mater. Chem. C* **2023**, *11*, 5657.

[83] G. Huang, C. Wang, S. Xu, S. Zong, J. Lu, Z. Wang, C. Lu, Y. Cui, *Adv. Mater.* **2017**, *29*, 1700095.

[84] R. Zhang, J. Qu, Z. Chen, C. Wang, S. Xu, *Appl. Phys. Express* **2021**, *14*, 051007.

[85] L. Jing, K. Ding, S. V. Kershaw, I. M. Kempson, A. L. Rogach, M. Gao, *Adv. Mater.* **2014**, *26*, 6367.

[86] N. Pradhan, S. Das Adhikari, A. Nag, D. D. Sarma, *Angew. Chemie - Int. Ed.* **2017**, *56*, 7038.

[87] S. Das Adhikari, S. K. Dutta, A. Dutta, A. K. Guria, N. Pradhan, S. Das Adhikari, S. K. Dutta, A. Dutta, A. K. Guria, N. Pradhan, *Angew. Chemie Int. Ed.* **2017**, *56*, 8746.

[88] C. Liu, J. Lin, W. Zhai, Z. Wen, X. He, M. Yu, Y. Huang, Z. Guo, C. Yu, C. Tang, *RSC Adv.* **2019**, *9*, 39315.

[89] P. Song, B. Qiao, D. Song, J. Cao, Z. Shen, Z. Xu, S. Zhao, S. Wageh, A. Al-Ghamdi, *ACS Appl. Mater. Interfaces* **2020**, *12*, 30711.

[90] T. He, J. Li, X. Qiu, S. Xiao, X. Lin, *Photonics Res.* **2018**, *6*, 1021.

[91] C.-C. Lin, T.-R. Liu, S.-R. Lin, K. M. Boopathi, C.-H. Chiang, W.-Y. Tzeng, W.-H. C. Chien, H.-S. Hsu, C.-W. Luo, H.-Y. Tsai, H.-A. Chen, P.-C. Kuo, J. Shiue, J.-W. Chiou, W.-F. Pong, C.-C. Chen, C.-W. Chen, *J. Am. Chem. Soc.* **2022**, *144*, 15718.

[92] Y. Zhao, C. Xie, X. Zhang, K. Matras-Postolek, P. Yang, *ACS Appl. Nano Mater.* **2021**, *4*, 6223.

[93] K. Justice Babu, G. Kaur, A. Shukla, A. Kaur, T. Goswami, N. Ghorai, H. N. Ghosh, *J. Phys. Chem. Lett.* **2021**, *12*, 302.

[94] Q. Y. Zhang, X. Y. Huang, *Prog. Mater. Sci.* **2010**, *55*, 353.

[95] M. Liu, G. K. Grandhi, S. Matta, K. Mokurala, A. Litvin, S. Russo, P. Vivo, *Adv. Photonics Res.* **2021**, *2*, 2000118.

[96] X. Luo, T. Ding, X. Liu, Y. Liu, K. Wu, *Nano Lett.* **2019**, *19*, 338.

[97] X. Shen, Z. Wang, C. Tang, X. Zhang, B. R. Lee, X. Li, D. Li, Y. Zhang, J. Hu, D. Zhao, F. Zhang, W. W. Yu, B. Dong, X. Bai, *Nano Lett.* **2023**, *23*, 82.

[98] H. Li, X. Liu, D. Zhou, B. Dong, L. Xu, X. Bai, H. Song, *Adv. Mater.* **2023**, 3479.

[99] Y.-J. Yu, C. Zou, W.-S. Shen, X. Zheng, Q.-S. Tian, Y.-J. Yu, C.-H. Chen, B. Zhao, Z.-K. Wang, D. Di, O. M. Bakr, L.-S. Liao, *Angew. Chemie Int. Ed.* **2023**, *17*, 955.

[100] A. V Sokolova, N. V Tepliakov, A. O. Ismagilov, D. A. Tatarinov, A. A. Kalinichev, A. V

Koroleva, E. V Zhizhin, M. A. Baranov, E. V Ushakova, A. P. Litvin, *J. Phys. Chem. C* **2022**, *126*, 20550.

[101] M. Zeng, F. Artizzu, J. Liu, S. Singh, F. Locardi, D. Mara, Z. Hens, R. Van Deun, *ACS Appl. Nano Mater.* **2020**, *3*, 4699.

[102] Y. Zhu, G. Pan, L. Shao, G. Yang, X. Xu, J. Zhao, Y. Mao, *J. Alloys Compd.* **2020**, *835*, 155390.

[103] T. Cai, J. Wang, W. Li, K. Hills-Kimball, H. Yang, Y. Nagaoka, Y. Yuan, R. Zia, O. Chen, *Adv. Sci.* **2020**, *7*, 1.

[104] M. Zeng, F. Locardi, D. Mara, Z. Hens, R. Van Deun, F. Artizzu, *Nanoscale* **2021**, *13*, 8118.

[105] W. Niu, R. Zhang, Z. Wang, F. Huang, D. Chen, *Adv. Phys. Res.* **2022**, 2200071.

[106] Z.-K. K. Tan, R. S. Moghaddam, M. L. Lai, P. Docampo, R. Higler, F. Deschler, M. Price, A. Sadhanala, L. M. Pazos, D. Credgington, F. Hanusch, T. Bein, H. J. Snaith, R. H. Friend, *Nat. Nanotechnol.* **2014**, *9*, 687.

[107] J. Song, J. Li, X. Li, L. Xu, Y. Dong, H. Zeng, *Adv. Mater.* **2015**, *27*, 7162.

[108] J. Song, L. Xu, J. Li, J. Xue, Y. Dong, X. Li, H. Zeng, *Adv. Mater.* **2016**, *28*, 4861.

[109] P. Cheng, K. Han, J. Chen, *ACS Mater. Lett.* **2023**, *5*, 60.

[110] Z. Liu, H. Yang, J. Wang, Y. Yuan, K. Hills-Kimball, T. Cai, P. Wang, A. Tang, O. Chen, *Nano Lett.* **2021**, *21*, 1620.

[111] D. Wu, B. Huo, Y. Huang, X. Zhao, J. Yang, K. Hu, X. Mao, P. He, Q. Huang, X. Tang, *Small* **2022**, *18*, 2106001.

[112] F. Zhong, Y. He, Y. Sun, F. Dong, J. Sheng, *J. Mater. Chem. A* **2022**, *10*, 22915.

[113] S. Kumar, J. Jagielski, N. Kallikounis, Y.-H. Kim, C. Wolf, F. Jenny, T. Tian, C. J. Hofer, Y.-C. Chiu, W. J. Stark, T.-W. Lee, C.-J. Shih, *Nano Lett.* **2017**, *17*, 5277.

[114] W. Chen, F. Zhang, C. Wang, M. Jia, X. Zhao, Z. Liu, Y. Ge, Y. Zhang, H. Zhang, *Adv. Mater.* **2021**, *33*, 2004446.

[115] K. Zhang, L. Cao, Y. Tang, Y. Yu, Y. Shen, B. Wang, W. Wang, Y. Li, J. Tang, *Laser Photon. Rev.* **2023**, *17*, 2200689.

[116] K. Wei, B. Liang, C. Sun, Y. Jiang, M. Yuan, *Small Struct.* **2022**, *3*, 2200063.

[117] H. Wang, F. Ye, J. Sun, Z. Wang, C. Zhang, J. Qian, X. Zhang, W. C. H. Choy, X. W. Sun, K. Wang, W. Zhao, *ACS Energy Lett.* **2022**, *7*, 1137.

[118] T. He, J. Li, X. Qiu, S. Xiao, C. Yin, X. Lin, *Adv. Opt. Mater.* **2018**, *6*, 1800843.

[119] J. Zhang, T. Jiang, X. Zheng, C. Shen, X. Cheng, *Opt. Lett.* **2017**, *42*, 3371.

[120] F. Zhou, X. Ran, D. Fan, S. Lu, W. Ji, *Adv. Opt. Mater.* **2021**, *9*, 1.

[121] J. Chen, W. Zhang, T. Pullerits, *Mater. Horizons* **2022**, *9*, 2255.

[122] F. Zhao, J. Li, X. Gao, X. Qiu, X. Lin, T. He, R. Chen, *J. Phys. Chem. C* **2019**, *123*, 9538.

[123] W. Shen, J. Chen, J. Wu, X. Li, H. Zeng, *ACS Photonics* **2021**, *8*, 113.

[124] I. D. Skurlov, W. Yin, A. O. Ismagilov, A. N. Tcypkin, H. Hua, H. Wang, X. Zhang, A. P.

Litvin, W. Zheng, *Nanomaterials* **2022**, *12*, 1.

[125] T. He, J. Li, C. Ren, S. Xiao, Y. Li, R. Chen, X. Lin, *Appl. Phys. Lett.* **2017**, *111*, 1.

[126] K. C. Nawrot, M. Sharma, B. Cichy, A. Sharma, S. Delikanli, M. Samoć, H. V. Demir, M. Nyk, *ACS Photonics* **2022**, *9*, 256.

[127] G. H. Ahmed, Y. Liu, I. Bravić, X. Ng, I. Heckelmann, P. Narayanan, M. S. Fernández, B. Monserrat, D. N. Congreve, S. Feldmann, *J. Am. Chem. Soc.* **2022**, *144*, 15862.

[128] S. K. Ha, W. Shcherbakov-Wu, E. R. Powers, W. Paritmongkol, W. A. Tisdale, *ACS Nano* **2021**, *15*, 20527.

[129] V. Pinchetti, A. Anand, Q. A. Akkerman, D. Sciacca, M. Lorenzon, F. Meinardi, M. Fanciulli, L. Manna, S. Brovelli, *ACS Energy Lett.* **2019**, *4*, 85.

[130] X. Li, S. Duan, H. Liu, G. Chen, Y. Luo, H. Ågren, *J. Phys. Chem. Lett.* **2019**, *10*, 487.

[131] D. E. Sommer, D. R. Gamelin, S. T. Dunham, *Phys. Rev. Mater.* **2022**, *6*, 025404.

[132] D. Ricciarelli, D. Meggiolaro, P. Belanzoni, A. A. Alothman, E. Mosconi, F. De Angelis, *ACS Energy Lett.* **2021**, *6*, 1869.

[133] H. Tao, T. Wu, M. Aldeghi, T. C. Wu, A. Aspuru-Guzik, E. Kumacheva, *Nat. Rev. Mater.* **2021**, *6*, 701.

[134] X. Chen, H. Lv, *NPG Asia Mater.* **2022**, *14*, 69.

[135] Y. A. Timkina, V. S. Tuchin, A. P. Litvin, E. V Ushakova, A. L. Rogach, *Nanomaterials* **2023**, *13*, 744.

[136] N. Chen, T. Cai, W. Li, K. Hills-Kimball, H. Yang, M. Que, Y. Nagaoka, Z. Liu, D. Yang, A. Dong, C. Y. Xu, R. Zia, O. Chen, *ACS Appl. Mater. Interfaces* **2019**, *11*, 16855.

[137] W. Gan, L. Cao, S. Gu, H. Lian, Z. Xia, J. Wang, *Chem. Mater.* **2023**, DOI: 10.1021/acs.chemmater.3c00446.

[138] P. Pansa-Ngat, K. Singh, B. Patel, C. Seriwattanachai, P. Kanjanaboos, O. Voznyy, *Chem. Mater.* **2023**, *35*, 271.